The acetylase activity of Cdu1 protects *Chlamydia* effectors from degradation to regulate bacterial exit from infected cells

Robert J. Bastidas[1*], Mateusz Kędzior[1], Lee Dolat[1], Barbara S. Sixt[2,3,4], Jonathan N. Pruneda[5], Raphael H. Valdivia[1,6*]

Author affiliations: [1]Department of Immunology, Duke University, Durham, N.C 27708, USA. [2]Deparment of Molecular Biology, Umeå University, Umeå, Sweden. [3]The Laboratory for Molecular Infection Medicine Sweden (MIMS), Umeå University, Umeå, Sweden. [4]Umeå Centre for Microbial Research (UCMR), Umeå University, Umeå, Sweden. [5]Department of Molecular Microbiology & Immunology, Oregon Health & Science University, Portland, OR 97239, USA. [6]Department of Molecular Genetics and Microbiology, Duke University, Durham, N.C 27708, USA.

* Correspondence: robert.bastidas@duke.edu; raphael.valdivia@duke.edu

Abstract

Many cellular processes are regulated by ubiquitin-mediated proteasomal degradation. Bacterial pathogens can regulate eukaryotic proteolysis through the delivery of proteins with de-ubiquitinating (DUB) activities. The obligate intracellular pathogen *Chlamydia trachomatis* secretes Cdu1 (ChlaDUB1), a dual deubiquitinase and Lys-acetyltransferase, that promotes Golgi remodeling and survival of infected host cells presumably by regulating the ubiquitination of host and bacterial proteins. Here we determined that Cdu1's acetylase but not its DUB activity is important to protect Cdu1 from ubiquitin-mediated degradation. We further identified three *C. trachomatis* proteins on the pathogen-containing vacuole (InaC, IpaM, and CTL0480) that required Cdu1's acetylase activity for protection from degradation and determined that Cdu1 and these Cdu1-protected proteins are required for optimal egress of *Chlamydia* from host cells. These findings highlight a non-canonical mechanism of pathogen-mediated protection of virulence factors from degradation after their delivery into host cells and the coordinated regulation of secreted effector proteins.

Introduction

Ubiquitination is a conserved and ubiquitous post-translational modification (PTM) of proteins involving the conjugation of the carboxy-terminal glycine residue of ubiquitin (Ub) to lysine residues of target proteins. Poly-ubiquitination of substrates involves further conjugation of a Ub internal lysine residue or amino-terminal methionine (M1) with a second Ub molecule. Seven internal lysines in Ub (K6, K11, K27, K29, K33, K48, K63) and M1 are utilized by Ub conjugating enzymes to form homogeneous, branched, or mixed poly-ubiquitin (polyUb) chains (Komander and Rape., 2012). PolyUb chains with different linkage types exhibit distinct structures and functions. For example, K48- and K11-linked polyUb chains exhibit a compact conformation and are substrates for 26S proteasome-mediated degradation (Varadan et al., 2004; Tenno et al., 2004; Eddins et al., 2007; Bremm et al., 2010; Saeki., 2017). In contrast, K63-linked polyUb

conjugates adopt more open conformations that enable the recruitment of multiprotein complexes that regulate the function of the target protein by proteolytic independent events (Komander et al., 2009b; Weeks et al., 2009; Datta et al., 2009; Komander and Rape., 2012). Mixed and branched polyUb chains are also emerging as important regulators of physiological functions (Swatek and Komander., 2016; Ohtake and Tsuchiya., 2017).

Protein ubiquitination regulates numerous eukaryotic cell processes including protein degradation, signal transduction, cell cycle regulation, selective autophagy, the DNA damage response, and programmed cell death. Ub also plays key roles in modulating host innate immune responses to bacterial infection (Li et al., 2016), bacterial proteins, pathogen-containing vacuoles, and bacteria themselves by targeting them for Ub-mediated degradation by proteasomal or autophagic machineries (Li et al., 2016). Because the Ub system is critical for pathogen containment, many pathogens have evolved mechanisms to counteract the impact of this PTM (Vozandychova et al., 2021). For instance, bacterial deubiquitinases (DUBs) can remove Ub from ubiquitinated substrates thereby dampening inflammatory and cell-autonomous defense mechanisms (Kubori et al., 2019). Many DUBs are cysteine proteases with a catalytic Cys, a nearby His and an Asn/Asp (Komander et al., 2009a). DUBs are typically dedicated to the removal of Ub moieties and are unable to hydrolyze other Ub-like (Ubl) modifications such as SUMO or NEDD8. However, the CE clan of Ubl proteases (ULPs) can catalyze the removal of both SUMO and NEDD8 (Ronau et al., 2016). Bacterial pathogens also encode CE clan enzymes that function as DUBs, ULPs or both. For instance, *Salmonella* Typhimurium SseL, *Escherichia coli* ElaD, and *Shigella flexneri* ShiCE function as Ub specific proteases (Rytkönen et al., 2007; Catic et al., 2007; Pruneda et al., 2016) while RickCE from *Rickettsia belli* functions as a protease directed towards both Ub and NEDD8 as does SidE from *Legionella pneumophila* which displays mixed activities towards Ub, NEDD8, and ISG15 (Sheedlo et al., 2015; Pruneda et al., 2016). Similarly, XopD from *Xanthamonas campestris* and LotB from *L. pneumophila* are

isopeptidases exhibiting cross reactivity towards both Ub and SUMO (Pruneda et al., 2016; Schubert et al., 2020). Some CE clan bacterial effectors display acetyltransferase activity. *L. pneumophila* LegCE, *S.* Typhimurium AvrA, and YopJ from *Yersinia pestis* function exclusively as acetyltransferases (Mittal et al., 2006; Mukherjee et al., 2006; Jones et al., 2008; Pruneda et al., 2016). In contrast, the *Chlamydia trachomatis* (Ct) effector Cdu1/*Chla*DUB1 is a CE clan protein that exhibits both acetyltransferase and deubiquitinating activities (Misaghi et al., 2006; Pruneda et al., 2016; Fischer et al., 2017; Pruneda et al., 2018).

Ct is an obligate intracellular bacterial pathogen responsible for human diseases of significant clinical and public health importance (Haggerty et al., 2010). Ct has a biphasic developmental cycle in which the Ct infectious propagule or elementary body (EB) invades the target host cell. Upon internalization the EB transitions to the reticulate body (RB). RBs replicate by binary fission within a pathogenic vacuole ("inclusion") and asynchronously differentiate back to EBs. In cell culture, starting at around 48 hours-post infection (hpi) Ct will egress after lysis of the host cell or by a process termed extrusion, wherein the entire inclusion is exocytosed from the infected cell (Moulder., 1991; Abdelrahman and Belland., 2005; Hybiske and Stephens., 2007; Lee et al., 2018). The effector Cdu1 was originally identified as a deneddylating and deubiquitinating enzyme and subsequently shown to exhibit *in-vitro* isopeptidase activity towards both Lys48 and Lys63 linked di-Ub substrates (Misaghi et al., 2006; Claessen et al., 2013; Pruneda et al., 2016; Fischer et al., 2017). Cdu1 is unique among CE clan enzymes in that it also functions as a bona fide lysine acetylase with both is acetylase and DUB activities catalyzed by the same catalytic active site (Pruneda et al., 2018). Intriguingly, Cdu1 autoacetylation is directed towards lysines unlike other CE clan acetylases that predominantly target serine and threonine residues (Pruneda et al., 2018). In infected cells, Cdu1 localizes to the inclusion membrane where it functions to stabilize the anti-apoptotic protein Mcl-1 and to promote the repositioning of Golgi ministacks around the Ct inclusion (Fischer et al., 2017;

Wang et al., 2018; Pruneda et al., 2018; Kunz et al., 2019; Auer et al., 2020). However, the mechanism by which Cdu1 promotes redeployment of Golgi ministacks and any additional roles that Cdu1 may play during Ct infection of epithelial cells remains unknown.

In this study, we show that Cdu1 protects itself and three secreted Ct effectors, InaC, IpaM, and CTL0480 from targeted ubiquitination and proteasomal degradation. InaC, IpaM, and CTL0480 are members of a larger family of bacterial proteins embedded within the inclusion membrane (Inc proteins) (Bannantine et al., 2000; Rockey et al., 2002; Chen et al., 2006; Li et al., 2008; Alzhanov et al., 2009; Dehoux et al., 2011; Lutter et al., 2012; Lutter et al., 2013; Kokes et al., 2015; Weber et al., 2015). We show that Cdu1-mediated protection from degradation is independent from its DUB activity but relies upon its Lys acetylase activity. We show that Cdu1 protects InaC to promote repositioning of Golgi ministacks and formation of actin scaffolds around the Ct inclusion, and CTL0480 to promote recruitment of myosin phosphatase target subunit 1 (MYPT1) to the inclusion. In addition, we determined that Cdu1 and Cdu1-protected Incs are required for optimal extrusion of inclusions from host cells at the late stages of infection.

Results

The *C. trachomatis* inclusion membrane proteins InaC, IpaM, and CTL0480 are differentially ubiquitinated in the absence of Cdu1

Cdu1 is required for Golgi repositioning around the Ct inclusion (Pruneda et al., 2018; Auer et al., 2020). To understand how Cdu1 promotes Golgi redistribution, we first generated a *cdu1* null strain in a Ct L2 (LGV L2 434 Bu) background by TargeTron mediated insertional mutagenesis (pDFTT3-*aadA*) (Lowden et al., 2015) (S. Figure 1). Loss of Cdu1 expression in the resulting L2 *cdu1*::GII *aadA* (*cdu1*::GII) strain was verified by western blot analysis and by

indirect immunofluorescence with antibodies raised against Cdu1 (S. Figures 2A and 2B). Because *cdu2* resides directly downstream of the *cdu1* locus and encodes a second Ct DUB (Cdu2/*Chla*DUB2) (Misaghi et al., 2006), we first determined whether the disruption of *cdu1* impacted the expression of *cdu2*. We detected *cdu1* and *cdu2* transcripts in HeLa cells infected with Ct L2 but not for the juncture between *cdu1* and *cdu2* (S. Figure 2C). In cells infected with Ct *cdu1*::GII we only detected *cdu2* transcripts (S. Figure 2C) confirming that *cdu1* and *cdu2* are not co-expressed as part of an operon in accordance with previous observations (Albrecht et al., 2010).

We hypothesized that Cdu1s' DUB activity promoted Golgi redistribution around inclusions and that we could identify potential targets by comparing the protein ubiquitination profile of cells infected with WT or *cdu1*::GII strains by quantitative mass spectrometry (MS). HeLa cell were mock infected or infected with either WT L2 or *cdu1*::GII strains. At 24 hpi, poly-ubiquitinated proteins were enriched from lysed cells using Tandem Ubiquitin Binding Entities (TUBEs) (LifeSensors). TUBEs consist of concatenated Ub binding associated domains (UBAs) that bind to polyUb-modified proteins with nanomolar affinities. Poly-ubiquitinated proteins of both human and Ct origin were enriched and identified by quantitative LC-MS/MS analysis.

Over 2,000 non-ubiquitinated proteins co-precipitated with TUBE 1 bound proteins across all three conditions (mock, L2, and *cdu1*::GII infected HeLa cells) and 3 biological replicates (S. Table 1). Among these, 47 human proteins were significantly enriched in mock infected HeLa cells and 50 human proteins were significantly enriched during Ct infection (L2 and *cdu1*::GII) (S. Table 3, S. Figure 3) Pathway enrichment analysis revealed that proteins involved in RNA metabolism were overrepresented among co-precipitating proteins from mock infected cells (S. Table 4, S. Figure 4) while no biological pathways or processes were overrepresented in

proteins enriched from infected cells (S. Figure 4). We also identified 8 TUBE1 co-precipitating Ct proteins in HeLa cells infected with L2 and *cdu1*::GII (S. Table 5, S. Figure 3).

TUBE 1 affinity capture lead to the identification of 43 ubiquitinated proteins (35 human proteins and 8 Ct proteins across all 3 conditions and replicates) based on the presence of peptides containing a di-glycine remnant motif (Peng et al., 2003) (S. Tables 6-8). The lack of widespread poly-ubiquitination of either human or Ct proteins in response to Ct infection (Figure 1) was surprising given that wholesale changes in protein ubiquitination has been reported during infection of HeLa cells by intracellular pathogens like *S.* Typhimurium (Fiskin et al., 2016). Only two human ubiquitinated proteins (ZC3H7A and DDIT4) were found to be significantly enriched in response to WT L2 infection (Figures 1A and 1C, S. Table 8) while only one human protein (MGC3121) was preferentially ubiquitinated in HeLa cells infected with the *cdu1*::GII mutant strain (Figures 1B and 1C, S. Table 8). In contrast three Ct proteins, InaC (K104, K107, and K149), IpaM (K29), and CTL0480 (K115) were ubiquitinated at Lys residues in the absence of Cdu1 (Figures 1B, 1C, and 1D, S. Table 8). InaC, IpaM, and CTL0480 are Ct effector proteins that localize to the inclusion membrane (Chen et al., 2006; Alzhanov et al., 2009; Lutter et al., 2013; Kokes et al., 2015). These Type 3 secretion substrates belong to a family of over 36 inclusion membrane proteins that contain a signature bi-lobal hydrophobic transmembrane domain (Bannantine et al., 2000; Rockey et al., 2002; Li et al., 2008; Dehoux et al., 2011; Lutter et al., 2012). Because Cdu1 also localizes to the inclusion membrane (Fischer et al., 2017; Wang et al., 2018; Pruneda et al., 2018; Kunz et al., 2019) we postulated that Cdu1 directly protects InaC, IpaM, and CTL0480 from ubiquitination.

Cdu1 associates with InaC, IpaM, and CTL0480

We first determined if Cdu1 co-localized with InaC, IpaM, and CTL0480 at the inclusion membrane. HeLa cells were infected for 24 hours with WT L2 or L2 expressing CTL0480-Flag

from its endogenous promoter and immunostained with antibodies against Cdu1, InaC, IpaM, or the Flag epitope. Both InaC and CTL0480-Flag localized throughout the inclusion membrane while IpaM was restricted to discrete microdomains as previously reported (Alzhanov et al., 2009; Dumoux et al., 2015) (Figure 2A). Cdu1 co-localized with InaC and CTL0480-Flag and with IpaM at microdomains (Figures 2A and 2B). All four antibodies specifically recognized their corresponding antigens since immunostaining for Cdu1, InaC, IpaM or the Flag epitope was not observed in Ct strains lacking Cdu1 (*cdu1*::GII), InaC (M407, Kokes et al., 2015) IpaM (*ipaM*::GII, Meier et al., 2022), or a strain that does not express CTL0480-Flag (Figure 2A).

We next determined if Cdu1 can interact with InaC, IpaM, and CTL0480 by co-transfecting HEK 293 cells with vectors expressing either full length Cdu1-GFP or truncated versions of Cdu1-GFP lacking transmembrane or catalytic domains (Figure 2C), and vectors expressing Flag-InaC, V5-IpaM, and V5-CTL0480. Transfected cells were lysed and Cdu1-GFP was immunoprecipitated with antibodies against GFP. Western blot analysis of the immunoprecipitates showed that Flag-InaC, V5-IpaM, and V5-CTL0480 co-precipitated with Cdu1-GFP (Figures 2D-F). Moreover, the transmembrane domain of Cdu1 was necessary for Cdu1-GFP to interact with all three Incs (Figures 2D-F). The interaction between Cdu1-GFP and the three tagged Incs was specific since we did not detect interactions between Cdu1-GFP and a V5-tagged version of the inclusion membrane protein CpoS (Sixt et al., 2017) (Figure 2G). We conclude from these results that Cdu1 can interact with all three Incs even in the absence of infection and that interactions are facilitated by the transmembrane domain of Cdu1.

Cdu1 protects InaC, IpaM, and CTL0480 proteins from degradation during infection

We next assessed if Cdu1 was required to stabilize endogenous InaC, IpaM, and CTL0480 in infected cells. HeLa cells were infected with either WT L2 or *cdu1*::GII strains and at various time points in the Ct infectious cycle crude cell lysates were analyzed by western blot to assess

the relative abundance of Inc proteins. At 24 hpi, we observed a decrease in InaC protein levels in cells infected with *cdu1*::GII relative to cells infected with WT L2 (Figure 3A). In contrast, IpaM protein levels did not decrease until 36 hpi in *cdu1*::GII infected cells (Figure 3B). For CTL0480, we were not able to detect CTL0480 by western blot but were successful in following CTL0480 expression by indirect immunofluorescence (Figure 3C). The relative abundance of CTL0480 at inclusion membranes, like IpaM, was not affected in *cdu1*::GII inclusions at 24 hpi. However, at 36 hpi, a subpopulation of cells lost CTL0480 immunoreactivity and by 48 hpi, inclusion membranes of the *cdu1*::GII strain were devoid of CTL0480 while CTL0480 was prominently detected at the inclusion membranes of WT L2 (Figures 3C and 3D). As controls for the specificity of antibodies used for western blots and for indirect immunofluorescence, we included cells infected with Ct lacking *ipaM (ipaM*::GII, Meier et al., 2022), with an *inaC* nonsense mutant (M407, Kokes et al., 2015), and with Ct lacking *ctl0480* (*ctl0480*::GII, Shaw et al., 2018). Overall, our results indicate that steady state protein levels of InaC and IpaM and CTL0480 localization at the inclusion membrane, especially at late stages of infection, are dependent on Cdu1, and that Cdu1 acts at different stages in the infection cycle.

The acetylase activity of Cdu1 is required for Cdu1 to protect itself, InaC, and IpaM from polyubiquitination and proteasomal degradation

The crystal structures of Cdu1 bound to Ub or Coenzyme A indicated that the adenosine and phosphate groups of Coenzyme A make contact with a helix in variable region 3 (VR-3) of Cdu1 while the Ile36-patch of Ub binds to the opposite face of the same helix (Pruneda et al., 2018). Although Cdu1 catalyzes both of its DUB and acetylase (Act) activities with the same active site (Pruneda et al., 2018) the two activities of Cdu1 can be uncoupled by the amino acid substitution K268E in VR-3 which disrupts Coenzyme A binding required for Act activity and by the amino acid substitution I225A in the Ub-binding region of VR-3 required for DUB activity

(Pruneda et al., 2018). These substitutions allowed us to test which of Cdu1's enzymatic functions are required for the observed effects on protein stability. We generated Ct shuttle plasmids (pBOMB4-MCI backbone), expressing WT Cdu1, a catalytically inactive variant of Cdu1 lacking both DUB and Act activities ($Cdu1^{C345A}$) (Pruneda et al., 2018), a Cdu1 DUB-deficient variant ($Cdu1^{I225A}$), and a Cdu1 Act-deficient variant ($Cdu1^{K268E}$). All Cdu1 constructs were expressed as 3X Flag epitope-tagged versions and from the Cdu1 endogenous promoter.

Plasmids expressing each Cdu1 variant were transformed into the *cdu*1::GII mutant and the resulting strains used to infect HeLa cells for 36 and 48 hours. The levels of endogenous InaC and IpaM in cell extracts of infected cells were monitored by western blot analysis. At 36 hpi, InaC protein levels drastically decreased in cells infected with *cdu1* null strains transformed with empty vector or expressing the catalytic inactive variant of Cdu1 ($Cdu1^{C345A}$-Flag) (Figure 4A). Likewise, IpaM protein levels diminished at 48 hpi during infection with the same strains (Figure 4B). Both InaC and IpaM protein levels were restored to wild type levels in *cdu1* null strains complemented with wild type Cdu1-Flag (Figures 4A and 4B). Unexpectedly, cells infected with a *cdu1* null strain ectopically expressing the DUB deficient Cdu1 variant ($Cdu1^{I225A}$-Flag) displayed wild type levels of InaC and IpaM while the Act deficient variant ($Cdu1^{K268E}$-Flag) did not (Figures 4A and 4B). These results suggest that the acetylase activity of Cdu1 rather than its DUB activity is required for Cdu1's ability to stabilize InaC and IpaM proteins.

When we monitored the stability of each Flag-tagged Cdu1 variant, we observed that the catalytically inactive variant of Cdu1 (C345A-Flag) was destabilized (Figures 4A and 4B- Flag WB). We reasoned that Cdu1 also protects itself from being targeted for degradation in infected cells. As with InaC and IpaM, the acetylase but not the DUB activity of Cdu1 was required for

Cdu1's stability (Figures 4A and 4B). Although the C345A (DUB-, Act-) and K268E (Act-) amino acid substitutions in Cdu1 do not destabilize Cdu1 expressed in *E. coli* (Pruneda et al., 2018), it was possible that these substitutions impacted the expression and/or folding of Cdu1 in *Chlamydia*. To determine if these Cdu1 mutants were inherently unstable, we expressed Cdu1^{C345A}-Flag and Cdu1^{K268E}-Flag in WT L2 in the presence of endogenous Cdu1. We found that each Flag-tagged variant was stabilized (Figure 4C), indicating that endogenous Cdu1 protected the catalytically-deficient Cdu1 variants *in trans*. In addition, western blot analysis of immunoprecipitated Cdu1-Flag and Cdu1^{C345A}-Flag expressed in a *cdu1*::GII mutant showed that while wild-type Cdu1-Flag was not modified by Lys48-linked poly-ubiquitination, Cdu1^{C345A}-Flag was robustly modified by Lys48-linked polyUb in the presence of the proteasome inhibitor MG132 (Figure 4D). Moreover, endogenous Cdu1 protected Cdu1^{C345A}-Flag from Lys48-linked polyUb when Cdu1^{C345A}-Flag was expressed in a wild type L2 background (Figure 4D). These results indicate that the loss of Cdu1 activity likely leads to its Lys48-linked poly-ubiquitination and subsequent proteasome-dependent degradation.

Because Cdu1 autoacetylates itself and its Act activity is directed towards lysines (Pruneda et al., 2018) we postulated that Cdu1 may stabilize proteins from degradation by acetylating lysine residues that are potential targets of ubiquitination. We tested this hypothesis by assessing whether Cdu1, InaC, CTL0480, and IpaM are acetylated at lysines during infection. Fractions enriched for inclusion membranes were isolated by sub-cellular fractionation from HeLa cells infected with wild-type L2 (24 hpi), and proteins acetylated at lysines were immunoprecipitated. Western blot analysis of acetyl-lysine immunoprecipitates indicated that InaC and IpaM, but not the Inc protein IncA, were acetylated (Figure 4E). Western blot analysis of anti-acetyl-lysine immunoprecipitates of inclusion membrane-enriched membrane fractions of HeLa cells infected

with L2 expressing Cdu1-Flag (24 hpi), CTL0480-Flag (40 hpi), and IpaM-Flag (40 hpi) also showed that all three Flag tagged effectors were acetylated at lysines (Figure 4F). We also determined that Flag-tagged InaC expressed in an M407 (*inaC* null) background was acetylated at lysines as determined by western blot analysis of anti-acetyl-lysine immunoprecipitates (Figure 4G). In addition, we identified acetylated forms of Cdu1 from mass spectrometric analysis of Flag immunoprecipitates derived from extracts of HeLa cells infected with L2 expressing Cdu1-Flag, (24 hpi) (Figure 4H).

We reasoned that the lysine acetylase activity of Cdu1 is a prominent mechanism by which Cdu1 protects client proteins (at 24 hpi), since loss of Cdu1 or expression of the acetylase deficient variant of Cdu1 (Cdu1^{K268E}-Flag) leads to a marked increase in Ub immunostaining at or near the periphery of *cdu1*::GII inclusions (> 80% of inclusions) compared to HeLa cells infected with *cdu1*::GII strains complemented with wild type or DUB deficient (I225A-Flag) Cdu1 strains (Figures 5A and 5B). Given that Cdu1 appears to localize exclusively at inclusion membranes we predicted that its activity would be spatially restricted to the inclusion periphery. We tested this premise by co-infecting HeLa cells with an *incA* null strain (M923 (IncA R197*), Kokes et al., 2015) and the *cdu1*::GII strain. IncA mediates homotypic fusion of inclusion membranes and loss of IncA results in the accumulation of multiple unfused inclusions in cells infected at high MOIs (Hackstadt et al., 1999; Suchland et al., 2000; Pannekoek et al., 2005) (Figure 5C). As expected, *incA* mutants which retain Cdu1 activity did not accumulate Ub at or near the periphery of inclusion membranes. In HeLa cells bearing both *cdu1*::GII and M923 inclusions, *cdu1::GII* Cdu1^{C345A} and M923 inclusions, or *cdu1*::GII Cdu1^{K268E} and M923 inclusions, only the M923 inclusions were protected from ubiquitination (Figures 5C and 5D). Based on these observations we conclude that the acetylase activity of Cdu1 protects proteins

in cis and that this activity is constrained to the membrane of the pathogenic vacuole consistent with previous reports (Auer et al., 2020).

Cdu1 is required for F-actin assembly and Golgi ministack repositioning around the Ct inclusion, and for MYPT1 recruitment to Ct inclusions

InaC is required for Ct to assemble F-actin scaffolds and to reposition Golgi mini stacks around the peripheries of inclusion membranes (Kokes et al., 2015; Wesolowski et al., 2017; Haines et al., 2021). Because Cdu1 regulates InaC levels, we predicted that *cdu1* mutants would phenocopy *inaC* mutants. We quantified the number of inclusions surrounded by F-actin cages at 40 hpi. In cells infected with Rif-R L2 (wild type parental strain of M407, Nguyen and Valdivia., 2012; Kokes et al., 2015), 25% of inclusions were surrounded by F-actin, consistent with previous observations (Chin et al., 2012; Kokes et al., 2015) (Figures 6A and 6E). The number of inclusions surrounded by F-actin decreased to 7% in cells infected with M407 (*inaC* null) and increased to 49% in HeLa cells infected with M407 complemented with wild type InaC (Figures 6A and 6E). A significant increase in inclusions surrounded by F-actin was also observed in host cells infected with *cdu1*::GII mutants expressing Cdu1-Flag and Cdu1^{I225A}-Flag (DUB-) (52% and 46% respectively) (Figures 6A and 6E) while *cdu1*::GII mutants transformed with an empty plasmid or expressing Cdu1^{C345A}-Flag (DUB- Act-) and Cdu1^{K268E}-Flag (Act-) resulted in only 8%,13%, and 10% of inclusions enveloped by F-actin respectively (Figures 6A and 6E). From these observations we conclude that the acetylase activity of Cdu1 is required for Ct to promote assembly of F-actin around the Ct inclusion likely through the stabilization of InaC.

We next quantified Golgi dispersal in infected HeLa cells at 24 hpi, a process that is also dependent on InaC (Kokes et al., 2015; Wesolowski et al., 2017). In Hela cells infected with an

inaC null strain (M407) Golgi dispersal was limited to only 26% of the Ct inclusion perimeter. In contrast, cells infected with either L2 Rif-R or with M407 complemented with wild type InaC, the Golgi is dispersed around 45% of the inclusion perimeter (Figures 6B and 6D). Similarly, Golgi dispersal around inclusions during infection with WT Ct L2 and in *cdu1*::GII mutants expressing wild type Cdu1-Flag or Cdu1^{I225A}-Flag (DUB-) was 43%, 41%, and 43% respectively (Figures 6B and 6D). In HeLa cells infected with *cdu1*::GII and *cdu1*::GII strains expressing Cdu1^{C345A}-Flag (DUB- Act-), and Cdu1^{K268E}-Flag (Act-), Golgi repositioning was restricted to only 24%, 23%, and 23% of inclusion perimeters respectively (Figures 6B and 6D). These results confirm that both InaC and Cdu1 are required for efficient repositioning of the Golgi around the Ct inclusion as previously reported (Kokes et al., 2015; Wesolowski et al., 2017; Pruneda et al., 2018; Auer et al., 2020) and that this process is independent of Cdu1's DUB activity but requires its acetylase activity. Moreover, our results suggest that Cdu1 promotes Golgi repositioning by protecting InaC-mediated redistribution of the Golgi around the Ct inclusion.

CTL0480 promotes recruitment of the myosin phosphatase subunit MYPT1 to the inclusion membrane where it regulates the extrusion of intact inclusions from host cells (Lutter et al., 2013; Shaw et al., 2018). Consistent with the gradual loss of CTL0480 from inclusions in cells infected with the *cdu1*::GII strain starting at 36 hpi (Figures 3C and 3D) we also observed a complete loss of MYPT1 recruitment to inclusions by 48 hpi (Figures 6C and 6F).

Cdu1, InaC, IpaM, and CTL0480 are required for optimal extrusion of Ct from host cells

In the absence of Cdu1, the levels of InaC, CTL0480, and IpaM decreased late in infection (36 hpi and 48 hpi, Figures 3 and 4) suggesting that a prominent role of Cdu1 is to protect these Incs from degradation late in infection. At the end of its developmental cycle, *Chlamydia* exits host cells by promoting cellular lysis or by extrusion of intact inclusions (Hybiske and Stephens.,

2007). Ct host cell exit by extrusion is an active process requiring a remodeling of the actin cytoskeleton and the function of Inc proteins (Hybiske and Stephens., 2007; Chin et al., 2012; Lutter et al., 2013; Shaw et al., 2018; Nguyen et al., 2018). CTL0480 recruits MYPT1 (an inhibitor of Myosin II motor complexes) to the inclusion membrane which prevents premature extrusion of Ct inclusions and loss of CTL0480 leads to increased rates of extrusion by Ct from infected HeLa cells (Lutter et al., 2013; Shaw et al., 2018) (Figure 7). Actin polymerization is also required for Ct extrusion (Hybiske and Stephens., 2007; Chin et al., 2012) suggesting that InaC dependent recruitment of F-actin to the inclusion may also contribute to optimal Ct extrusion. IpaM localizes to microdomains in the inclusion membrane that are proposed to function as foci for extrusion (Nguyen et al., 2018). Based on these observations, we postulated that Cdu1-mediated protection of CTL0480, InaC, and IpaM regulates the extrusion of Ct inclusions. We quantified the number of extrusions released from infected HeLa cells at 52 hpi and observed a 60% reduction in the number of extrusions in HeLa cells infected with the *cdu1*::GII strain relative to cells infected with WT L2 (Figures 7A and 7B). Complementation of *cdu1*::GII with either wild type Cdu1-Flag or Cdu1^{I225A}-Flag (DUB-) restored extrusion production to near wild type levels. Infection of HeLa cells with *inaC* (*inaC*::GII, Wesolowski et al., 2017), or *ipaM* (*ipaM*::GII, Meier et al., 2020) null strains led to a 75% and 58% reduction in extrusion production respectively (Figures 7A and 7B). Impaired extrusion of inclusions by *cdu1*::GII, *inaC*::GII, and *ipaM*::GII strains was not due to defects in inclusion biogenesis, since all three strains produced similar number of inclusions at 48 hpi relative to cells infected with WT L2 (Supp. Figure 5). We conclude that Cdu1, InaC, and IpaM function to promote optimal extrusion of Ct inclusions from host cells.

In contrast, infection of HeLa cells with a *ctl0480::GII* mutant strain led to an increase in the number of extruded inclusions as previously observed (Shaw et al., 2018) (Figures 7A and 7B).

Therefore, even though the Cdu1-mediated protection of InaC and IpaM is important for the extrusion of inclusions and *cdu1* mutants phenocopy the loss of InaC and IpaM, the phenotypic similarities do not extend to the increased number of extruded inclusions observed in cells infected with the *ctl0480*::GII mutant strain (Figures 7A and 7B). We infer from these observations that functions for both InaC and IpaM in the extrusion of inclusions are epistatic to CTL0480. Extruded inclusions produced during infection of HeLa cells also varied in size with an average diameter of 40 μm (Figures 7A and 7C). Interestingly, the loss of IpaM and over expression of Cdu1-Flag and Cdu1^{I225A}-Flag (DUB-) shifted the size distribution of extrusions toward larger extrusions (Figures 7A and 7C) suggesting that Ct regulates the size of extruded inclusions through Cdu1.

Discussion

Several *Chlamydia* effector proteins localize to the inclusion membrane to regulate interactions between the *Chlamydia* pathogenic vacuole and the host cytoskeleton, organelles, and vesicular trafficking pathways. They also modulate host cell death programs and promote *Chlamydia* exit from host cells (reviewed in Bugalhão and Mota., 2019)**.** Given the central roles that Incs play in promoting *Chlamydia* intracellular infection, it is not surprising that they are targeted for inactivation by host cellular defenses. In response, *Chlamydia* has evolved mechanisms to protect Incs. In this study we show that the acetylase activity of the effector Cdu1 protects itself as well as three independent Incs; InaC, IpaM, and CTL0480, from ubiquitination and degradation (Figure 8). Interestingly, all three Incs play prominent roles in regulating the extrusion of *Chlamydia* inclusions from host cells (Figure 7). Observations that the encapsulation of *Chlamydia* within an extruded inclusion enhances survival of *Chlamydia* within macrophages (Zuck et al., 2017) together with the broad conservation of extrusion as an exit strategy among *Chlamydia* (Zuck et al., 2016) suggests that this mechanism is important for

Chlamydia pathogenesis. Thus, targeting *Chlamydia* Incs that regulate extrusion for Ub-mediated destruction may be advantageous for the host. In this context, we hypothesize that InaC is targeted for degradation due to its role in promoting F-actin assembly around the inclusion, since F-actin is essential for extrusion (Hybiske and Stephens., 2013; Chin et al., 2012). However, other roles of InaC like its regulation of microtubule scaffolds around the inclusion cannot be ruled out (Wesolowski et al., 2017; Haines et al., 2021). CTL0480 was previously shown to function as an inhibitor of extrusions through its role in modulating the activity of myosin light chain 2 (MLC_2) (Lutter et al., 2013; Shaw et al., 2018). IpaM localizes to specialized microdomains in the inclusion membrane which are also sites of enrichment for over 9 inclusion membrane proteins including CTL0480 and MrcA, both of which are required for *Chlamydia* extrusion (Mital et al., 2010; Lutter et al., 2013; Nguyen et al., 2018). IpaM is a third inclusion membrane protein localizing to microdomains that is required for the optimal extrusion of inclusions and lends support to a potential role for microdomains as foci for extrusion (Nguyen et al., 2018). We also find that the loss of IpaM shifted the size distribution of extrusions towards larger inclusions indicating that Ct constraints the size of extruded inclusions (Figure 7). We speculate that heterogeneity in the size of extrusions might facilitate uptake of some extrusions by innate immune cells at infected mucosal sites. Uptake of *Chlamydia* by host phagocytes has been proposed to promote *Chlamydia* LGV dissemination to distal sites in the genital tract to avoid clearance of *Chlamydia* by other immune cells (Zuck et al., 2017). Protection of IpaM by Cdu1 could therefore be advantageous for *Chlamydia* EBs within extrusions to escape to distal sites and avoid exposure to localized inflammatory responses.

Effectors that modulate the activity of other translocated effectors are referred to as “metaeffectors”, a term coined by Kubori and colleagues after observing that the *L. pneumophila* effector LubX which functions as an E3 ligase, ubiquitinates the translocated effector SidH leading to its degradation (Kubori et al., 2010). Several other effector-metaeffector interactions

429 have been described in *L. pneumophila*, *Salmonella enterica*, and *Brucella abortus* which
430 regulate the activity of other effectors either directly or indirectly by modifying the same host
431 target or cellular process (Kubori et al., 2010; Neunuebel et al., 2011; Jeong et al., 2015;
432 Urbanus et al., 2016; Smith et al., 2020; Iyer and Das., 2021). In this context Cdu1 functions as
433 an atypical metaeffector since it targets multiple effectors and unlike other effector-metaeffector
434 pairs it is not encoded in the same locus as its targets. We also observed that Cdu1 interactions
435 with InaC, IpaM, and CTL0480 likely occur independently from each other and that the
436 stoichiometry and kinetics of degradation varies for each Inc during infection of host cells. For
437 example, InaC protein levels decrease as early as 24 hpi while IpaM and CTL0480 protein
438 levels decrease at later stages of infection (36 and 48 hpi) (Figure 3). Furthermore, in the
439 absence of Cdu1, we observe almost complete loss of InaC at 36 hpi (Figure 4A) and of
440 CTL0480 at 48 hpi (Figures 3C and 3D), while only a subpopulation of IpaM is destabilized
441 throughout infection (Figures 3B and 4B).
442
443 The observation that the DUB activity of Cdu1 was not required to protect InaC, IpaM, and
444 CTL0480 from ubiquitination was unexpected and pointed to a potential role for its acetylation
445 activity instead. Because Cdu1 can interact with InaC, IpaM, and CTL0480 we hypothesized
446 that Cdu1 may protect these Incs through acetylation of lysine residues that are otherwise
447 targeted for ubiquitination. Indeed, we found that all three Incs and Cdu1 are acetylated at
448 lysines in infected cells, however, we were unable to determine if lysine acetylation in all four
449 proteins was dependent on Cdu1s' Act activity or if these PTMs are protective. Why the DUB
450 activity of Cdu1 is unable to compensate for loss of its Act activity remains unknown. It is
451 possible that Cdu1, like other DUBs, is regulated by PTMs (Komander et al., 2009a). For
452 instance, phosphorylation of human CYLD inhibits its DUB activity towards TRAF2 while
453 phosphorylation of human USP8 inhibits its DUB activity toward EGFR (Reiley et al., 2005;
454 Mizuno et al., 2007). Mass spectrometry analysis of immunoprecipitated Flag tagged Cdu1

expressed in Ct revealed that Cdu1 is phosphorylated at multiple serine and threonine residues (Figure 4H) as previously suggested (Zadora et al., 2019). We identified three PX(S/T)P MAPK phosphorylation consensus sequence motifs in the proline rich domain (PRD) of Cdu1, suggesting that MAPKs may regulate the DUB activity of Cdu1.

Cdu1 homologs are found in multiple *Chlamydia* species including *C. trachomatis*, *C. muridarum*, *C. suis*, *C. psitacci*, *C. abortus*, *C. caviae*, and *C. felis* but is notably absent in the genomes of *C. pneumoniae* and *C. pecorum*. The acquisition of a second deubiquitinase paralog (Cdu2) has also occurred in *C. trachomatis*, *C. muridarum*, and *C. suis*. In the genomes of all three species, *cdu2* resides directly adjacent to *cdu1*; an arrangement that presumptively arose from a gene duplication event. Cdu2 is a dedicated ULP with deubiquitinating and deneddylating activities (Misaghi et al., 2006; Pruneda et al., 2016). New evidence suggest that both paralogues might not be functionally redundant. The crystal structure of Cdu2 has revealed differences in residues involved in substrate recognition between Cdu1 and Cdu2 and that each paralog might recognize polyUb chains differently (Hausman et al., 2020). The processivity rates for removal of terminal Ub from polyUb chains also differs between both isopeptidases with Cdu2 exhibiting limited trimming of polyUb as compared to Cdu1 (Hausman et al., 2020). Moreover, Cdu2 lacks the proline rich domain found in Cdu1 which might be important for regulation of Cdu1 enzymatic activity. The presence of Cdu2 might also explain the low incidence of human and Ct proteins that were differentially ubiquitinated in the absence of Cdu1 (Figure 1). Whereas several *Chlamydia* species have acquired either one or two deubiquitinase paralogs, both *C. pneumoniae* and *C. pecorum* have not. Instead, both species have acquired an unrelated deubiquitinase (*Chla*OTU) belonging to the OTU family of proteases (Makarova et al., 2000; Furtado et al., 2013). Curiously, *Chla*OTU is also found in *C. psitacci*, *C. abortus*, *C. caviae*, and *C. felis* all of which encode only Cdu1 and is absent in *C. trachomatis*, *C. muridarum*, and *C. suis*, all of which encode Cdu1 and Cdu2. It is noteworthy that *Chlamydi*a

species have independently acquired deubiquitinases multiple times (Cdu1, Cdu2, *Chla*OTU) and that some of these deubiquitinases have evolved into moonlighting enzymes reflecting the diverse strategies adopted by pathogenic *Chlamydia* as they adapt to their particular niche.

Acknowledgements

We thank LifeSensors and the Duke Proteomics and Metabolomics Shared Resource Center for their proteomics services. We thank the Duke Light Microscopy Core Facility for microscopy services. We also thank Marcela Kokes for generating the IncA-Flag constructs used in this study. This work was supported by NIH grants AI140019 to R.J.B and AI134891 to R.H.V.

Author contributions

R.J.B and R.H.V designed the study. R.J.B wrote the manuscript with input from all listed authors. L.D generated the *cdu1*::GII strain. M.K verified generation of the *cdu1*::GII mutant strain and showed interaction of Cdu1-GFP variants with InaC, IpaM, and CTL0480 in transfected HEK cells. R.J.B performed all other experiments. B.S.S and J.N.P shared reagents. R.J.B and R.H.V proofed the manuscript.

Declaration of interests

R.H.V is a founder of Bloom Sciences (San Diego, CA), which is a microbiome therapeutics company. Findings reported in this study are unrelated to the work being performed with Bloom Sciences.

Material and Methods

Key Resource Table

REAGENT or RESOURCE	SOURCE	IDENTIFIER
Antibodies		

See S. Table 9		
Bacterial and virus strains		
Chlamydia trachomatis LGV biovar L2 434 Bu (L2)	Richard Stephens (UC Berkeley)	N/A
L2 pBOMB-MCI (Parent: LGV L2 434 Bu)	This paper	N/A
L2 pBOMB-MCI_CTL0480-3XFlag (Parent: LGV L2 434 Bu)	This paper	N/A
L2 pBOMB-MCI_IpaM-3XFlag (Parent: LGV L2 434 Bu)	This paper	N/A
L2 pBOMB-MCI_Cdu1-3XFlag (Parent: LGV L2 434 Bu)	This paper	N/A
L2 pBOMB-MCI_Cdu1 ^{C345A}-3XFlag (Parent: LGV L2 434 Bu)	This paper	N/A
L2 pBOMB-MCI_Cdu1 ^{K268E}-3XFlag (Parent: LGV L2 434 Bu)	This paper	N/A
L2 *cdu1*::GII *aadA* (Parent: LGV L2 434 Bu)	This paper	N/A
L2 *cdu1*::GII *aadA* pBOMB-MCI (Parent: L2 *cdu1*::GII *aadA*)	This paper	N/A
L2 *cdu1*::GII *aadA* pBOMB-MCI_Cdu1-3XFlag (Parent: L2 *cdu1*::GII *aadA*)	This paper	N/A
L2 *cdu1*::GII *aadA* pBOMB-MCI_Cdu1 ^{C345A}-3XFlag (Parent: L2 *cdu1*::GII *aadA*)	This paper	N/A
L2 *cdu1*::GII *aadA* pBOMB-MCI_Cdu1 ^{I225A}-3XFlag (Parent: L2 *cdu1*::GII *aadA*)	This paper	N/A
L2 *cdu1*::GII *aadA* pBOMB-MCI_Cdu1 ^{K268E}-3XFlag (Parent: L2 *cdu1*::GII *aadA*)	This paper	N/A
L2 Rif-R (Parent: L2 434 Bu)	Nguyen et al., 2012	N/A
M407 (*inaC C307T*, InaC Q103*) (Parent: L2 Rif-R)	Kokes et al., 2015	N/A
M407 p2TK2 (Parent: M407)	Kokes et al., 2015	N/A
M407 p2TK2_InaC (Parent: M407)	Kokes et al., 2015	N/A
M407 p2TK2_InaC-3X Flag (Parent: M407)	This paper	N/A
inaC::GII *bla* (Parent: L2 434 Bu)	Wesolowski et al., 2017	N/A
ipaM::GII *cat* (Parent: L2 434 Bu)	Meier et al., 2022	N/A
ctl0480::GII *aadA* (Parent: L2 434 Bu)	Shaw et al., 2018	N/A
M923 (*incA C589T*, IncA R197*) (Parent: L2 Rif-R)	Kokes et al., 2015	N/A
M923 pBOMB-MCI (Parent: M923)	Sixt et al., 2017	N/A
Biological samples		
N/A		
Chemicals, peptides, and recombinant proteins		
PR-619 (DUB inhibitor)	Sigma-Aldrich	Cat# SML0430

MG132 (proteasome inhibitor)	Sigma-Aldrich	Cat# 474791
TUBE-1 (pUb affinity capture reagent)	LifeSensors	Cat# UM401M
Acti-stain™ 488 (Phalloidin 488)	Cytoskeleton Inc.	Cat# PHDG1
ChromoTek GFP-Trap® Agarose	Proteintech	Cat# gta
Protein A/G PLUS-Agarose	Santa Cruz Biotechnology	Cat# sc-2203
3xFLAG peptide	APExBIO	Cat# A6001
LGV L2 434 Bu Cdu1 recombinant protein	Jonathan Pruneda (Oregon Health and Science University)	N/A
Critical commercial assays		
TargeTron™ gene knockout system	Sigma-Aldrich	Cat# TA0100
Deposited data		
C. trachomatis LGV L2 434 Bu proteome	NCBI	NCBI:txid47472
Homo sapiens (Human) proteome	UniProt	Proteome ID: UP000005640
TUBE-1 affinity capture proteomics data	PRIDE	To be deposited
Cdu1 lysine acetylation proteomic data	PRIDE	To be deposited
Experimental models: Cell lines		
Hela cells	ATCC	Cat# CCL-2 RRID:CVCL_0030
Vero cells	ATCC	Cat# CCL-81 RRID:CVCL_0059
HEK 293T cells	ATCC	Cat# CRL-3216 RRID:CVCL_0063
Experimental models: Organisms/strains		
Chlamydia trachomatis LGV L2 434 Bu	Richard Stephens (UC Berkeley)	N/A
Oligonucleotides		
See S. Table 10		
Recombinant DNA		
Plasmid: pDFTT3-aadA_Cdu1 635/636	This paper	N/A
Plasmid: pOPIN-GFP_Cdu1 FL (aa 1-401)	Jonathan Pruneda (Oregon Health and Science University)	N/A
Plasmid: pOPIN-GFP_Cdu1 TMD- (aa 71-401)	Jonathan Pruneda (Oregon Health and Science University)	N/A
Plasmid: pOPIN-GFP_Cdu1 CD- (aa 1-130)	Jonathan Pruneda (Oregon Health and Science University)	N/A
Plasmid: pCDNA-DEST53 (w/o GFP)_InaC (CT813)-3XFLAG	This paper	N/A
Plasmid: pcDNA3.1/nV5-DEST_IpaM	This paper	N/A
Plasmid: pcDNA3.1/nV5-DEST_CTL0480 p	This paper	N/A
Plasmid: pcDNA3.1/nV5-DEST_CpoS	This paper	N/A
Plasmid: pBOMB4-MCI_CTL0480-3X Flag	This paper	N/A
Plasmid: pBOMB4-MCI_IpaM-3X Flag	This paper	N/A
Plasmid: pBOMB4-MCI_Cdu1-3XFlag	This paper	N/A
Plasmid: pBOMB4-MCI_Cdu1 C345A-3XFlag	This paper	N/A

Plasmid: pBOMB4-MCI_Cdu1 I225A-3XFlag	This paper	N/A
Plasmid: pBOMB4-MCI_Cdu1 K263E-3XFlag	This paper	N/A
Plasmid: p2TK2_SW2_InaC-3XFlag	This paper	N/A
Software and algorithms		
Targetronics	Targetronics, LLC	www.targetrons.com
Proteome Discoverer 2.3	Thermo Fisher Scientific	https://www.thermofisher.com/us/en/home/industrial/mass-spectrometry/liquid-chromatography-mass-spectrometry-lc-ms/lc-ms-software/multi-omics-data-analysis/proteome-discoverer-software.html
Mascot software	Matrix Science	https://www.matrixscience.com
MaxQuant 1.6.2.3		https://www.maxquant.org
Scaffold PTM	Proteome Software	https://www.proteomesoftware.com/products/scaffold-ptm
VolcaNoseR	Goedhart, and Luijsterburg., 2020	https://huygens.science.uva.nl/VolcaNoseR/
Metascape	Zhou et al., 2019	https://metascape.org/gp/index.html#/main/step1
DAVID Bioinformatic Resources	Huang et al., 2009a., Huang et al., 2009b	https://david.ncifcrf.gov/tools.jsp
Image J	Schneider et al., 2012	https://imagej.nih.gov/ij/
NEBaseChanger	New England Biolabs	https://nebasechanger.neb.com
Prism 9	GraphPad	https://www.graphpad.com/updates/prism-900-release-notes
Other		
N/A		

Resource Availability

Materials availability

- All newly generated materials associated with this study will be freely available upon request.

Data and code availability

- Proteomics data will be deposited at PRIDE (Proteomics Identification Database-EMBL-EBI) and publicly available at the time of publication. Accession numbers will be listed in the key resources table.

- Original data used for microscopy and western blots in this study will be deposited online (Mendeley data) and made available at the time of publication.

- Any additional information required to reanalyze the data reported in this paper is available upon request.

- This paper does not report original code.

Experimental Model And Subject Details

Cell lines

Vero (CCL-81; RRID:CVCL_0030), HeLa (CCL-2; RRID:CVCL_0059), and HEK293T (CRL-3216; CVCL_0063) cells were purchased from ATCC and cultured in High Glucose Dulbecco's Modified Eagle's Medium supplemented with L-glutamine, sodium pyruvate (DMEM; Gibco) and 10% fetal bovine serum (FBS; Sigma-Aldrich). Cells were grown at 37°C in a 5% CO2 humidified incubator. Vero, Hela, and HEK293T cells were derived from females. All three cell lines have been authenticated by the Duke Cell Culture and DNA analysis facility.

Chlamydia strains and propagation

Chlamydia strains used in this study are listed in the Key Resources Table. Ct strains were propagated in Vero cells and harvested by osmotic lysis at 48 hours post infection. Following lysis extracts were sonicated and bacteria pelleted by centrifugation at 21,000 x g. Bacteria were resuspended in SPG storage buffer (75g/L sucrose, 0.5 g/L KH_4HPO_4, 1.2 g/L Na_2HPO_4, 0.72 g/L glutamic acid, pH 7.5) and stored as single use aliquots at -80°C.

Method Details

***Chlamydia* infections**

Chlamydia infections were synchronized by centrifugation (2,500 x *g* for 30 minutes at 10°C) onto HeLa cell monolayers and incubated for the indicated times. Co-infections were performed by infecting HeLa cell monolayers at a 1:1 ratio using MOIs of 2 for each co-infecting strain.

Insertional mutagenesis of CTL0247 (*cdu1*)

Primer sequences for TargeTron™ mediated mutagenesis of the LGV L2 434 Bu *cdu1* (CTL0247) ORF were designed at the TARGETRONICS, LLC web portal (www.targetrons.com). IBS1/2, EBS1/delta, and EBS2 primers (primer sequences are listed in S. Table 10) were used in a PCR reaction to generate homing sequences for TargeTron™ integration between nucleotides 635 and 636 of the *cdu1* ORF using a TargeTron™ gene knockout system (Sigma-Aldrich; TA0100) according to the manufacturer instructions. Homing sequences were gel purified, digested with HindIII and BsrGI, and ligated into HindIII and BsrGI digested pDFTT3-*aadA* (Lowden et al., 2015). Ligations were transformed into *E. coli* DH5α, clones isolated, and *cdu1* redirected pDFTT3-aadA plasmids identified by restriction digest and verified by Sanger sequencing (Eton Bioscience) using a T7-promoter specific primer. The resulting plasmid was transformed into a *C. trachomatis* LGV L2 434 Bu strain and transformants selected with 150 μg/mL spectinomycin and plaque purified as previously

560 described (Kędzior and Bastidas., 2019). Insertion of the GII *aadA* intron at the *cdu1* locus was
561 verified by PCR analysis (S. Figure1) using primers that amplify amplicons spanning the
562 *cdu1*::GII 5' (RBP409 and RBP436) and 3' (RBP468 and RBP118) junctions, the *cdu1* CDS
563 (RBP409 and RBP118), and the *aadA* CDS (RBP512 and RBP513). Primer sequences are
564 listed in S. Table 10. Loss of Cdu1 protein was verified by western blot and indirect
565 immunofluorescence analysis (S. Figures 2A and 2B).
566
567 **Analysis of *cdu1* and *cdu2* transcription by RT-PCR**
568 Confluent HeLa cell monolayers (2.9 x 10^6 cells/infection) were infected with wild type L2 434
569 Bu or L2 *cdu1*::GII *aadA* strains. At 24 hpi, total RNA was isolated with a Qiagen RNeasy kit
570 (Qiagen; 74004) according to the manufacturer instructions. Total RNA was treated twice with
571 DNAse I (NEB; M0303S) and used for cDNA synthesis using a SuperScript IV Reverse
572 Transcriptase kit (Thermo Fisher Scientific; 18090010). cDNAs synthesized with and without
573 reverse transcriptase were used as templates for PCR analysis (S. Figure 2C) using primers
574 that amplify amplicons spanning the *cdu*1 (CTL0247_F and CTL0247_R) and *cdu2* ORFs
575 (CTL0246_F and CTL0247_R), and the intergenic junction between the *cdu1* and *cdu2* ORFs
576 (CTL0246-0247_F and CTL0246-0247_R). Primer sequences can be found in the S. Table 10.
577
578 **TUBE1 based global ubiquitin profiling**
579 Confluent HeLa cell monolayers (5.04 x 10^6 cells/infection) were mock infected or separately
580 infected with WT LGV L2 434 Bu or a L2 *cdu1*::GII *aadA* strain at MOIs of 3. At 24 hpi cells were
581 collected and spun down (700 x *g* for 10 minutes), frozen at -80°C and shipped on dry ice to
582 LifeSensors (Malvern, PA) for quantitative TUBE1-based Mass Spectrometry Analysis. Cell
583 pellets from three independent biological replicates were sent to LifeSensors for analysis. Cell
584 were subsequently lysed in lysis buffer (50 mM Tris-HCL, pH 7.5, 150 mM NaCl, 2 mM EDTA,
585 1% NP-40, 10% glycerol, 1% Sodium Deoxycholate) supplemented with a protease inhibitor

cocktail, the DUB inhibitor PR-619 (Sigma-Aldrich; SML0430), and the proteasomal inhibitor MG-132 (Sigma-Aldrich; 474791). Lysates were clarified by high-speed centrifugation (14,000 x *g*, 10 minutes, 4°C) and supernatants containing 5 mg of protein were equilibrated with magnetic TUBE-1 (LifeSensors; UM401M) and incubated overnight at 4°C under rotation. TUBEs were isolated with a magnetic stand and washed sequentially with PBST and TUBE wash buffer. Poly-ubiquitinated and associated proteins were eluted with TUBE elution buffer. Eluted supernatants were neutralized with neutralization buffer and loaded onto SDS-gels and run until SDS buffer reached 0.5 cm into the gel. Gels were stained with Coomassie Blue and lanes excised, reduced with TCEP, alkylated with iodoacetamide, and digested with Trypsin (Trypsin Gold, Mass Spectrometry Grade) (Promega; V5280). Tryptic digests were analyzed using a 150 min LC run on a Thermo Scientific™ Q Exactive HF Orbitrap™ LC-MS/MS system. MS data was searched against the UniProt human database (UniProt; Proteome ID: UP000005640) and the *Chlamydia trachomatis* L2 434 Bu reference database (NCBI:txid47472) using MaxQuant 1.6.2.3 (https://www.maxquant.org). Proteins, peptides, and site identification was set to a false discovery rate of 1%. N-terminal acetylation, Met oxidation, and diGly remnant on lysine residues was also identified. All peptides and proteins identified can be found in S. Table 1. The intensities (sum of all peptide MS peak areas for a protein or ubiquitinated peptide) for each protein and ubiquitinated peptide across all three biological replicates were used to determine mean intensities and to calculate *p*-values based on one-way student t-tests. Volcano plots of mean intensities vs. *p*-values were generated with VolcaNoseR (Goedhart and Lujsterburg., 2020) (https://huygens.science.uva.nl/VolcaNoseR/) and used to identify significantly enriched proteins and ubiquitinated peptides. Data used to generate each Volcano plot can be found in S. Table 2. Pathway enrichment analysis was performed with Metascape (Zhou et al., 2019) (https://metascape.org/gp/index.html#/main/step1) and DAVID bioinformatic resources (Huang et al., 2009a; Huang et al., 2009b) (https://david.ncifcrf.gov/tools.jsp).

Inhibitors, antibodies, and western blots

MG-132 (25 μM) (Sigma-Aldrich; 474791) was added to infected cell monolayers 5 hours prior to extract preparations. Recombinant Cdu1 protein (LGV L2 434 Bu, amino acids 71-401) was generated as previously described (Pruneda et al., 2018) and kindly provided by Jonathan Pruneda (Oregon Health and Science University, OR). Recombinant Cdu1 protein was used to generate antibodies in immunized New Zealand White rabbits. Cdu1 antisera was pre-adsorbed with crude cell extracts from HeLa cells infected with a *cdu1*::GII *aadA* strain. Pre-adsorbed antisera was used for western blot analysis at a 1:500 dilution in a solution containing 5% BSA supplemented with crude extracts from HeLa cells infected with a *cdu1*::GII *aadA* strain (0.1mg/mL total protein). Antibodies, antibody dilutions, and antibody diluents used in this study are listed in S. Table 9. For western blot analysis, lysates from infected HeLa cell monolayers (2.4×10^6 cells) were prepared by incubating cell monolayers with boiling hot 1% SDS lysis buffer (1% SDS, 100 mM NaCl, 50 mM Tris, pH 7.5). Lysates were collected, briefly sonicated, and total protein concentration measured with a DC™ Protein Assay Kit (BIO-RAD; 5000111). 8 μg (Slc1 and alpha Tubulin blots) and 25 μg of total protein lysates (all other blots) were loaded onto 4-15% Mini-PROTEAN and TGX Stain Free™ Protein Gels (BIO-RAD; 4568084), transferred to PVDF membranes (BIO-RAD; 1620177), blocked with 5% Milk/TBSt, and incubated with primary antibodies overnight at 4°C. Protein signals were detected with Goat anti mouse (H+L) IgG (ThermoFisher scientific; 31430) or Goat anti rabbit (H+L) IgG HRP (ThermoFisher scientific; 31460) conjugated secondary antibodies (1:1000 in 5% Milk/TBSt) and SuperSignal West Femto HRP substrate (ThermoFisher scientific; 34096). Antibody bound membranes were imaged with a LI-COR imaging system (LI-COR, Inc.). Varying amounts of protein extracts were used to determine the linear range of detection for InaC, IpaM, and Slc1

antibodies prior to quantification of western blot images with LI-COR imaging software (data not shown).

Immunofluorescence microscopy

HeLa cells were grown on coverslips to 50% confluency (0.1 x 10^5 cells) and infected at MOIs of 0.6. At indicated times, infected cells were separately fixed with ice cold Methanol or with warm PBS containing 4% formaldehyde for 20 minutes. After fixative removal, cells were washed with PBS and formaldehyde fixed cells were incubated either in 5% BSA/PBS supplemented with 0.1% Triton X-100 or in 5% BSA/PBS supplemented with 0.05% Saponin for 30 minutes with gentle rocking. Following washing with PBS, Methanol fixed cells were incubated with primary antibodies diluted in 5% BSA/PBS and formaldehyde fixed cells were incubated with primary antibodies diluted in 5% BSA/PBS supplemented with 0.1% Triton X-100 or 0.05% Saponin for 1 hour with gentle rocking. Dilutions for each antibody used can be found in S. Table 9. Methanol fixed cells were washed with PBS and incubated with secondary antibodies diluted in 5% BSA/PBS and supplemented with Hoechst 33342 (2 µg/mL) (ThermoFisher Scientific; H3570). Formaldehyde fixed cells were washed and incubated with 5% BSA/PBS supplemented with 0.1% Triton X-100 and Hoechst or 0.05% Saponin and Hoechst for 1 hour protected from light and with gentle rocking. For detection of F-actin, Phalloidin conjugated to Alexa Fluor™ 488 (1:5000) (Act-Stain 488 Phalloidin; Cytoskeleton Inc.; PHDG1) was added for the last 20 minutes of incubation with the secondary antibodies. Coverslips were transferred to glass slides, mounted with 10 µL of Vectashield (Vector Labs; H-1000) and incubated over night at room temperature prior to imaging. Secondary antibodies used were goat anti-mouse (H+L) IgG (ThermoFisher scientific; A-11001 and A-21235) and goat anti-rabbit (H+L) IgG (ThermoFisher scientific; A-11008 and A-21244) conjugated to Alexa Fluor™ 488 and Alexa Fluor™ 647. All of

659 the antibodies used for indirect immunofluorescence analysis were analyzed under all three
660 staining conditions (Methanol, Formaldehyde/Triton X-100, and Formaldehyde/Saponin).
661
662 Representative images were acquired with an inverted confocal laser scanning microscope
663 (Zeiss 880) equipped with an Airyscan detector (Hamamatsu) and with diode (405 nm), argon
664 ion (488 nm), double solid-state (561 nm) and helium-neon (633) lasers. Images were acquired
665 with a 63x C-Apochromatic NA 1.2 oil-objective (Zeiss). Images acquired in Airyscan mode were
666 deconvoluted using automatic Airyscan processing in Zen software (Zeiss). Image acquisition
667 was performed at the Light Microscopy Core Facility at Duke University. Images used for
668 quantification were captured in an inverted microscope (Ti2-Nikon instruments) equipped with
669 an ORCA Flash 4.0 V3 sCMOS camera (Hamamatsu) and a SOLA solid-state white light
670 illuminator (Lumencro). Images were acquired using a 60x Plan Apochromatic NA 1.40 oil
671 objective. All images were opened with ImageJ (Schneider et al., 2012) and only linear
672 adjustments were made to fluorescence intensity for the entire image. Images were exported as
673 TIFFs and compiled with Adobe suite software (Illustrator).
674
675 **Vector construction and *C. trachomatis* transformation**
676 *Constructs used in co-transfection experiments:* Mammalian vectors expressing Cdu1-GFP
677 constructs were kindly provided by Jonathan Pruneda (Oregon Health and Science University,
678 OR). Briefly, geneblocks encoding full length Cdu1 (LGV L2 434 Bu, CTL0247) (amino acids 1-
679 401), Cdu1 lacking its transmembrane domain (amino acids 71-401), and Cdu1 lacking its
680 catalytic domain (amino acids 1-130) were generated and inserted into the pOPIN-GFP vector
681 (Berrow et al., 2007) by In-Fusion™ cloning (Takara Bio; 638947), resulting in Cdu1 constructs
682 with a C-terminal eGFP-His tag preceded by a 3C protease cleavage site. The Flag-InaC
683 mammalian expression vector was derived from a Gateway™ entry clone containing the *C.*
684 *trachomatis* Serovar D/UW-3/CX CT813 (*inaC*) ORF (amino acids 41-264) obtained from a *C.*

trachomatis ORFeome library (Roan et al., 2006). The entry vector was used as a donor plasmid for Gateway™ based transfer into a modified pcDNA™ DEST53 (ThermoFisher Scientific; 12288015) vector in which the cycle 3 *GFP* ORF was removed. A NEB Q5®-Site Directed Mutagenesis Kit (New England Biolabs; E0554S) was used to introduce a 3X Flag epitope tag at the N-terminus of the CT813 ORF and a stop codon at the end of the CT813 ORF. L2 *ipaM* (CTL0476), L2 CTL0480, and L2 *cpoS* (CTL0481) ORFs were PCR amplified from cell lysates derived from Vero cells infected with wild type L2 LGV 434 Bu with primers containing attB sequences (primers *ipaM* forward, *ipaM* reverse, CTL0480 forward, CTL0480 reverse, *cpoS* forward, and *cpoS* reverse). Primer sequences can be found in the S. Table 10. PCR amplicons were used as donors for Gateway™ BP Clonase™ based transfers into the donor vector pDONR™221 (ThermoFisher Scientific; 12536017) to generate entry plasmids. Entry plasmids were used to transfer *ipaM*, CTL0480, and *cpoS* into the Gateway™ destination vector pcDNA™3.1/nV5-DEST (ThermoFisher Scientific; 12290010) by Gateway™ LR Clonase™ based reactions. The resulting mammalian expression vectors express IpaM, CTL0480, and CpoS with V5-epitopes fused to their N-terminus.

pBOMB4-MCI based plasmids. CTL0480 and *ipaM* ORFs were amplified by PCR from cell extracts derived from Vero cells infected with wild type LGV L2 434 Bu. The CTL0480 ORF, 149 b.p of upstream sequence, and a 3X FLAG epitope was amplified by PCR using primers RBP628 and RBP629. The CTL0476 (*ipaM*) ORF, 400 b.p of upstream sequence, and a 3X FLAG epitope was amplified with primers RBP623 and RBP624. CTL0480 and *ipaM* amplicons were digested with Not1 and Pst1 and cloned into Not1 and Pst1 digested pBOMB4-MCI (Bauler and Hackstadt., 2014) to generate pBOMB4-MCI_CTL0480-3X Flag and pBOMB4-MCI_IpaM-3X Flag plasmids respectively. pBOMB4-MCI_Cdu1-3XFlag plasmids were generated by PCR amplification of 175 b.p of genomic sequence directly upstream of the L2 434 Bu CTL0247 (*cdu1*) ORF and the entire *cdu1* ORF tagged with a C-terminal 3X Flag

epitope tag (primers RBP460 and RBP461). PCR amplicons were generated from gradient purified LGV L2 434 Bu EBs and cloned into a pCR™-Blunt II TOPO® vector using a Zero Blunt™ TOPO™ PCR cloning Kit (ThermoFisher Scientific; K2800J10) according to the manufacturer instructions. Cdu1 catalytic variants were generated with a NEB Q5®-Site Directed Mutagenesis Kit (New England Biolabs; E0554S) using the *cdu1*p-*cdu1*-3X Flag construct cloned into pCR™-Blunt II TOPO® as a template and following the manufacturer instructions. Primers for introducing base pair changes were designed on the NEBaseChanger website (https://nebasechanger.neb.com). The Cdu1^{C345A} variant was generated by changing the *TGC* codon located at positions 1033-1035 in the *cdu1* ORF to *GCT* (primers RBP525 and RBP526). The Cdu1^{I225A} variant was generated by substituting the *ATC* codon located at positions 673-675 for *GCT* (primers RBP527and RBP528). The Cdu1^{K268E} variant was generated by introducing an *A802G* base pair substitution (primers RBP529 and RBP530). Wild type *cdu1*p-*cdu1*-3XFLAG and all three *cdu1* variants were digested with Not1 and Pst1 and ligated into Not1 and Pst1 digested pBOMB4-MCI (Bauler and Hackstadt., 2014). Primer sequences can be found in the S. Table 10.

p2TK2_SW2-inaC-3XFlag. The CTL0184 (*inaC*) ORF and 250 b.p of upstream sequence was amplified by PCR from cell extracts derived from Vero cells infected with L2 434 Bu and cloned into the p2TK2_SW2 vector (Agaisse and Derré., 2013). A NEB Q5®-Site Directed Mutagenesis Kit (New England Biolabs; E0554S) was used to insert a 3X FLAG epitope sequence at the C-terminus (stop codon removed) of the CTL0184 ORF to generate the p2TK2_SW2-InaC-3XFlag plasmid.

pBOMB4-MCI based plasmids and p2TK2_SW2-InaC-3X Flag plasmids were transformed into corresponding *Chlamydia* strains, and transformants were selected with 10 U/mL Penicillin G

and plaque purified as previously described (Kędzior and Bastidas., 2019). All primer sequences and plasmids generated in this study are listed in S. Table 10 and Key Resources Table.

Subcellular fractionation

HeLa cells (2.16 x 10^7 cells/strain) seeded in six well plates were mock infected or infected with *Chlamydia* L2 434 Bu strains. At indicated time points cells were washed with ice-cold PBS, collected in ice-cold PBS with a cell scraper, and transferred to 15 mL conical tubes. Cell suspensions were centrifuged at 500 x g for 5 minutes at 4°C and cell pellets were resuspended in 400 µL of ice-cold subcellular fractionation buffer (20 mM HEPES (pH 7.4), 10 mM KCl, 2mM $MgCl_2$, 1mM EDTA, 1mM EGTA) supplemented with 1mM DTT and a 1x cOmplete Mini-EDTA free protease inhibitor cocktail (Sigma-Aldrich; 11836170001). Cells were incubated on ice for 20 minutes and lysed with 30 strokes of a Dounce homogenizer. Cell lysates were sequentially centrifuged twice at 720 x g for 5 minutes at 4°C to remove intact nuclei. Supernatants were centrifuged at 10,000 x g for 5 minutes at 4°C and the heavy membrane (inclusion) fraction was recovered and resuspended in IP lysis buffer (25 mM Tris-Hcl, 150 mM NaCl, 1% NP-40, 5% Glycerol) supplemented with 1mM PMSF and a 1x cOmplete Mini-EDTA free protease inhibitor cocktail (Sigma-Aldrich; 11836170001).

Immunoprecipitations (IPs)

Transfections and GFP-immunoprecipitations: HEK 293T cell monolayers (1.32 x 10^7 cells/transfection) seeded in 10 cm cell culture dishes pre coated with poly-L-Lysine (Sigma-Aldrich; P4707) were grown to 50% confluency and transfected with 10 µg of each plasmid used per co-transfection in a 1.5 to 1 ratio of jetOPTIMUS® (Polyplus; 101000051) transfection reagent to total plasmid DNA according to the manufacturer instructions. At 24 hpi, transfected

761 cells were lysed in IP lysis buffer (described above) supplemented with 1mM PMSF and 1x
762 cOmplete Mini-EDTA free protease inhibitor cocktail (Sigma-Aldrich; 11836170001). Lysates
763 were transferred to Eppendorf tubes, sonicated, and cleared by centrifugation (21,000 x *g*, 15
764 minutes, 4°C). Supernatants containing 2 mg of total protein were incubated with magnetic
765 GFP-Trap® agarose (Proteintech; gta) for 1 hour at 4°C with rotation. Beads were washed
766 according to manufacturer instructions and immunoprecipitated proteins eluted with 2X Laemmli
767 sample buffer.
768
769 *Flag immunoprecipitations*: Mock and infected HeLa cell monolayers (1.44 x 10^7 cells) grown in
770 six well plates were lysed in IP lysis buffer (described above) and transferred to Eppendorf
771 tubes. Lysates were sonicated and cleared by centrifugation (21,000 x *g*, 15 minutes, 4°C).
772 Supernatants containing 2 mg of total protein were pre-cleared by incubating with Protein A/G
773 PLUS-Agarose (Santa Cruz Biotechnology; sc-2203) for 30 minutes at 4°C followed by
774 sedimentation of agarose resins by centrifugation. Supernatants were incubated with M2-anti
775 Flag mouse mAb (1:400) (Sigma-Aldrich; F1804) overnight at 4°C with rotation followed by
776 incubation with Protein A/G PLUS-Agarose for 3 hours at 4°C with rotation. Agarose resins were
777 sedimented and washed according to manufacturer instructions and immunoprecipitated
778 proteins eluted with 50 μL of 100 μg/mL 3xFLAG peptides (APExBIO; A6001).
779
780 *Acetylated lysine immunoprecipitations*. Heavy membrane (inclusion) subcellular fractions
781 isolated from infected HeLa cells and containing 1 mg of total protein were pre-cleared by
782 incubating with Protein A/G PLUS-Agarose (Santa Cruz Biotechnology; sc-2203) for 30 minutes
783 at 4°C followed by sedimentation of agarose resins by centrifugation. Supernatants were
784 incubated with an anti-acetylated lysine rabbit antibody (Cell signaling; #9441) (1:100) overnight
785 at 4°C with rotation followed by incubation with Protein A/G PLUS-Agarose for 3 hours at 4°C

786 with rotation. Agarose resins were sedimented and washed according to manufacturer
787 instructions and immunoprecipitated proteins eluted with 50 µL of 2X Laemmli sample buffer.
788
789 Input (8 µg of total protein for Slc1 and alpha Tubulin blots, and 25 µg for all other blots) and
790 immunoprecipitates (GFP, Flag, proteins acetylated at lysines) were loaded onto 4-15% Mini-
791 PROTEAN and TGX Stain Free™ Protein Gels (BIO-RAD; 4568084), transferred to
792 PVDF membranes (BIO-RAD; 1620177), blocked with 5% Milk/TBSt, and incubated with
793 primary antibodies overnight at 4°C. Protein signals were detected with Goat anti mouse (H+L)
794 IgG (ThermoFisher scientific; 31430) or Goat anti rabbit (H+L) IgG HRP (ThermoFisher
795 scientific; 31460) conjugated secondary antibodies (1:1000 in 5% Milk/TBSt) and SuperSignal
796 West Femto HRP substrate (ThermoFisher scientific; 34096). Antibody bound membranes were
797 imaged with a LI-COR imaging system (LI-COR, Inc.).
798
799 **Identification Cdu1 lysine acetylation and phosphorylation sites by LC-MS/MS**
800 HeLa cell monolayers (8.64 x10^7 cells/strain) grown in six well plates were infected with a wild
801 type L2 strain transformed with empty pBOMB4-MCI (Bauler and Hackstadt., 2014) plasmid or
802 with a wild type L2 strain transformed with a pBOMB4-MCI_*cdu1*-3X Flag plasmid. At 24 hpi
803 infected cells were lysed and Flag tagged Cdu1 was immunoprecipitated as described above.
804 Flag eluates from 3 independent biological replicates were sent to the Proteomics and
805 Metabolomics Shared Resource Facility at Duke University for quantitative LC-MS/MS analysis.
806 Samples were spiked with undigested casein, reduced with 10 mM dithiothreitol, and alkylated
807 with 20 mM iodoacetamide. Eluates were then supplemented with 1.2% phosphoric acid and S-
808 Trap (Protifi) binding buffer (90% Methanol, 100 mM TEAB). Proteins were trapped on the S-
809 Trap, digested with 20 ng/µL Trypsin (Trypsin Gold, Mass Spectrometry Grade) (Promega;
810 V5280), and eluted with 50 mM TEAB, 0.2% FA, and 50% ACN/0.2% FA. Samples were

lyophilized and resuspended in 1% TFA/2% acetonitrile containing 12.5 fmol/μL yeast alcohol dehydrogenase. Quantitative LC/MS/MS was performed using a nanoAcquitiy UPLC system (Waters Corp) coupled to Thermo Scientific™ Orbitrap™ Fusion Lumos high resolution accurate mass tandem mass spectrometer via a nanoelectrospray ionization source. Data was analyzed with Proteome Discoverer 2.3 (Thermo Fisher Scientific™.) and MS/MS data searched against the *Chlamydia trachomatis* LGV L2 434 Bu reference database (NCBI:txid47472). Cdu1-Flag MS/MS data was analyzed with Mascot software (Matrix Science) using Trypsin/P specificity for N-terminal acetylation, lysine acetylation, lysine Ub, and S/T/Y phosphorylation identification. Analysis identified multiple acetylated and phosphorylated Cdu1 peptides and no Cdu1 ubiquitinated peptides. Data was viewed in Scaffold with Scaffold PTM (Scaffold Software).

Isolation and imaging of *Chlamydia* inclusion extrusions

HeLa cell monolayers (1.2 x 10^6 cells) were infected with Ct strains at MOIs of 0.8. At 48 hpi, infected monolayers were imaged using an EVOS FL Cell Imaging System (ThermoFisher Scientific) equipped with a 20x/0.4 NA objective and a CCD camera. Following imaging, growth media was removed, cell monolayers washed with fresh growth media, and monolayers incubated for an additional 4 hours at 37°C. At 52 hpi growth supernatants were collected and transferred to Eppendorf tubes. Extrusions were enriched by centrifugation (1,500 rpm, 5 min) and pellets (not always visible) containing extrusions were resuspended in 30 μL of 4% Formaldehyde/PBS supplemented with Hoechst (2 μg/mL) and 0.2% Trypan Blue Solution (Gibco, 0.4%). Extrusions were analyzed by plating 10 μL drops on a glass side (without coverslips) and immediately imaged using an EVOS FL Cell Imaging System (ThermoFisher Scientific) equipped with a 20x/0.4 NA objective and a CCD camera. Intact extrusions were identified based on morphology, lacking nuclei, and being impermeable to trypan blue. Images were opened in ImageJ (Schneider et al., 2012) and enumeration of inclusions and extrusions

was performed manually. The sizes of individual extrusions and inclusions were determined by manually tracing a line around the perimeter of each extrusion and inclusion in ImageJ and measuring perimeter length. All measurements were exported to Microsoft Excel. Data plots and statistical analyses were done with Prism 9 (GraphPad) software. Datasets were analyzed for significance using a paired student t-test.

Image analysis

Line scan profiles of Cdu1 co-localization with inclusion membrane proteins was performed with ImageJ (Schneider et al., 2012) by tracing a line through regions of interest and plotting fluorescent signal intensities with the Plot Profile function. Localization of CTL0480, recruitment of MYPT1, and association of Ub with Ct inclusions was performed manually from maximum projections in ImageJ. Assessment of F-actin recruitment to Ct inclusions was performed manually in ImageJ by projecting four to five sections in order to capture the entire inclusion. Redistribution of Golgi around the Ct inclusion was measured in ImageJ from maximum projections. The perimeters of individual inclusions were manually traced, and lengths measured. The length of dispersed Golgi was measured by tracing and measuring the length of the GM130 signal directly adjacent to each inclusion. Dispersed Golgi length was divided by inclusion perimeter length. All measurements were exported to Microsoft Excel for quantification. Data plots and statistical analyses were done with Prism 9 (GraphPad).

Quantification And Statistical Analysis

Quantifications were generated from three independent experiments and measurements derived from blinded images. Data plots and statistical analyses were done with Prism 9 (GraphPad) software. Datasets were analyzed for significance using a paired student t-test or one-way ANOVAs with a Student-Newman-Keuls post hoc test. Data graphs show means and

error bars represent standard error. *p*-values less than 0.05 are defined as statistically significant. The indicated statistical test for each experiment can be found in the figure legends.

References

1. Abdelrahman YM, Belland RJ. 2005. The chlamydial developmental cycle. *FEMS Microbiol Rev* **29**:949–959. doi:10.1016/j.femsre.2005.03.002

2. Agaisse H, Derré I. 2013. A *C. trachomatis* cloning vector and the generation of *C. trachomatis* strains expressing fluorescent proteins under the control of a *C. trachomatis* promoter. *PLoS ONE* **8**:e57090. doi:10.1371/journal.pone.0057090

3. Albrecht M, Sharma CM, Reinhardt R, Vogel J, Rudel T. 2010. Deep sequencing-based discovery of the *Chlamydia trachomatis* transcriptome. *Nucleic Acids Res* **38**:868–877. doi:10.1093/nar/gkp1032

4. Alzhanov DT, Weeks SK, Burnett JR, Rockey DD. 2009. Cytokinesis is blocked in mammalian cells transfected with *Chlamydia trachomatis* gene CT223. *BMC Microbiol* **9**:2. doi:10.1186/1471-2180-9-2

5. Auer D, Hügelschäffer SD, Fischer AB, Rudel T. 2020. The chlamydial deubiquitinase Cdu1 supports recruitment of Golgi vesicles to the inclusion. *Cell Microbiol* **22**:e13136. doi:10.1111/cmi.13136

6. Bannantine JP, Griffiths RS, Viratyosin W, Brown WJ, Rockey DD. 2000. A secondary structure motif predictive of protein localization to the chlamydial inclusion membrane. *Cell Microbiol* **2**:35–47. doi:10.1046/j.1462-5822.2000.00029.x

7. Bauler LD, Hackstadt T. 2014. Expression and targeting of secreted proteins from *Chlamydia trachomatis*. *J Bacteriol* **196**:1325–1334. doi:10.1128/JB.01290-13

8. Berrow NS, Alderton D, Sainsbury S, Nettleship J, Assenberg R, Rahman N, Stuart DI, Owens RJ. 2007. A versatile ligation-independent cloning method suitable for high-throughput expression screening applications. *Nucleic Acids Res* **35**:e45. doi:10.1093/nar/gkm047

9. Bremm A, Freund SMV, Komander D. 2010. Lys11-linked ubiquitin chains adopt compact conformations and are preferentially hydrolyzed by the deubiquitinase Cezanne. *Nat Struct Mol Biol* **17**:939–947. doi:10.1038/nsmb.1873

10. Bugalhão JN, Mota LJ. 2019. The multiple functions of the numerous *Chlamydia trachomatis* secreted proteins: the tip of the iceberg. *Microb Cell* **6**:414–449. doi:10.15698/mic2019.09.691

11. Catic A, Misaghi S, Korbel GA, Ploegh HL. 2007. ElaD, a Deubiquitinating protease expressed by *E. coli*. *PLoS ONE* **2**:e381. doi:10.1371/journal.pone.0000381

12. Chen C, Chen D, Sharma J, Cheng W, Zhong Y, Liu K, Jensen J, Shain R, Arulanandam B, Zhong G. 2006. The hypothetical protein CT813 is localized in the *Chlamydia trachomatis*

inclusion membrane and is immunogenic in women urogenitally infected with *C. trachomatis*. *Infect Immun* **74**:4826–4840. doi:10.1128/IAI.00081-06

13. Chen Y-S, Bastidas RJ, Saka HA, Carpenter VK, Richards KL, Plano GV, Valdivia RH. 2014. The *Chlamydia trachomatis* type III secretion chaperone Slc1 engages multiple early effectors, including TepP, a tyrosine-phosphorylated protein required for the recruitment of CrkI-II to nascent inclusions and innate immune signaling. *PLoS Pathog* **10**:e1003954. doi:10.1371/journal.ppat.1003954

14. Chin E, Kirker K, Zuck M, James G, Hybiske K. 2012. Actin recruitment to the *Chlamydia* inclusion is spatiotemporally regulated by a mechanism that requires host and bacterial factors. *PLoS ONE* **7**:e46949. doi:10.1371/journal.pone.0046949

15. Claessen JHL, Witte MD, Yoder NC, Zhu AY, Spooner E, Ploegh HL. 2013. Catch-and-release probes applied to semi-intact cells reveal ubiquitin-specific protease expression in *Chlamydia trachomatis* infection. *Chembiochem* **14**:343–352. doi:10.1002/cbic.201200701

16. Datta AB, Hura GL, Wolberger C. 2009. The structure and conformation of Lys63-linked tetraubiquitin. *J Mol Biol* **392**:1117–1124. doi:10.1016/j.jmb.2009.07.090

17. Dehoux P, Flores R, Dauga C, Zhong G, Subtil A. 2011. Multi-genome identification and characterization of chlamydiae-specific type III secretion substrates: the Inc proteins. *BMC Genomics* **12**:109. doi:10.1186/1471-2164-12-109

18. Dumoux M, Menny A, Delacour D, Hayward RD. 2015. A *Chlamydia* effector recruits CEP170 to reprogram host microtubule organization. *J Cell Sci* **128**:3420–3434. doi:10.1242/jcs.169318

19. Eddins MJ, Varadan R, Fushman D, Pickart CM, Wolberger C. 2007. Crystal structure and solution NMR studies of Lys48-linked tetraubiquitin at neutral pH. *J Mol Biol* **367**:204–211. doi:10.1016/j.jmb.2006.12.065

20. Fischer A, Harrison KS, Ramirez Y, Auer D, Chowdhury SR, Prusty BK, Sauer F, Dimond Z, Kisker C, Hefty PS, Rudel T. 2017. *Chlamydia trachomatis*-containing vacuole serves as deubiquitination platform to stabilize Mcl-1 and to interfere with host defense. *eLife* **6**. doi:10.7554/eLife.21465

21. Fiskin E, Bionda T, Dikic I, Behrends C. 2016. Global analysis of host and bacterial ubiquitinome in response to *Salmonella* Typhimurium infection. *Mol Cell* **62**:967–981. doi:10.1016/j.molcel.2016.04.015

22. Furtado AR, Essid M, Perrinet S, Balañá ME, Yoder N, Dehoux P, Subtil A. 2013. The chlamydial OTU domain-containing protein *Chla*OTU is an early type III secretion effector targeting ubiquitin and NDP52. *Cell Microbiol* **15**:2064–2079. doi:10.1111/cmi.12171

23. Gehre L, Gorgette O, Perrinet S, Prevost M-C, Ducatez M, Giebel AM, Nelson DE, Ball SG, Subtil A. 2016. Sequestration of host metabolism by an intracellular pathogen. *eLife* **5**:e12552. doi:10.7554/eLife.12552

24. Goedhart J, Luijsterburg MS. 2020. VolcaNoseR is a web app for creating, exploring, labeling and sharing volcano plots. *Sci Rep* **10**:20560. doi:10.1038/s41598-020-76603-3

25. Hackstadt T, Scidmore-Carlson MA, Shaw EI, Fischer ER. 1999. The *Chlamydia trachomatis* IncA protein is required for homotypic vesicle fusion. *Cell Microbiol* **1**:119–130. doi:10.1046/j.1462-5822.1999.00012.x

26. Haggerty CL, Gottlieb SL, Taylor BD, Low N, Xu F, Ness RB. 2010. Risk of sequelae after *Chlamydia trachomatis* genital infection in women. *J Infect Dis* **201 Suppl 2**:S134-55. doi:10.1086/652395

27. Haines A, Wesolowski J, Ryan NM, Monteiro-Brás T, Paumet F. 2021. Cross Talk between ARF1 and RhoA Coordinates the Formation of Cytoskeletal Scaffolds during *Chlamydia Infection*. *MBio* **12**:e0239721. doi:10.1128/mBio.02397-21

28. Hausman JM, Kenny S, Iyer S, Babar A, Qiu J, Fu J, Luo Z-Q, Das C. 2020. The Two Deubiquitinating Enzymes from *Chlamydia trachomatis* Have Distinct Ubiquitin Recognition Properties. *Biochemistry* **59**:1604–1617. doi:10.1021/acs.biochem.9b01107

29. Huang DW, Sherman BT, Lempicki RA. 2009a. Bioinformatics enrichment tools: paths toward the comprehensive functional analysis of large gene lists. *Nucleic Acids Res* **37**:1–13. doi:10.1093/nar/gkn923

30. Huang DW, Sherman BT, Lempicki RA. 2009b. Systematic and integrative analysis of large gene lists using DAVID bioinformatics resources. *Nat Protoc* **4**:44–57. doi:10.1038/nprot.2008.211

31. Hybiske K, Stephens RS. 2007. Mechanisms of host cell exit by the intracellular bacterium *Chlamydia*. *Proc Natl Acad Sci USA* **104**:11430–11435. doi:10.1073/pnas.0703218104

32. Iyer S, Das C. 2021. The unity of opposites: Strategic interplay between bacterial effectors to regulate cellular homeostasis. *J Biol Chem* **297**:101340. doi:10.1016/j.jbc.2021.101340

33. Jeong KC, Sexton JA, Vogel JP. 2015. Spatiotemporal regulation of a *Legionella pneumophila* T4SS substrate by the metaeffector SidJ. *PLoS Pathog* **11**:e1004695. doi:10.1371/journal.ppat.1004695

34. Jones RM, Wu H, Wentworth C, Luo L, Collier-Hyams L, Neish AS. 2008. *Salmonella avra* coordinates suppression of host immune and apoptotic defenses via JNK pathway blockade. *Cell Host Microbe* **3**:233–244. doi:10.1016/j.chom.2008.02.016

35. Kędzior M, Bastidas RJ. 2019. Forward and reverse genetic analysis of *Chlamydia*. *Methods Mol Biol* **2042**:185–204. doi:10.1007/978-1-4939-9694-0_13

36. Kokes M, Dunn JD, Granek JA, Nguyen BD, Barker JR, Valdivia RH, Bastidas RJ. 2015. Integrating chemical mutagenesis and whole-genome sequencing as a platform for forward and reverse genetic analysis of *Chlamydia*. *Cell Host Microbe* **17**:716–725. doi:10.1016/j.chom.2015.03.014

37. Komander D, Clague MJ, Urbé S. 2009a. Breaking the chains: structure and function of the deubiquitinases. *Nat Rev Mol Cell Biol* **10**:550–563. doi:10.1038/nrm2731

38. Komander D, Reyes-Turcu F, Licchesi JDF, Odenwaelder P, Wilkinson KD, Barford D. 2009b. Molecular discrimination of structurally equivalent Lys 63-linked and linear polyubiquitin chains. *EMBO Rep* **10**:466–473. doi:10.1038/embor.2009.55

39. Komander D, Rape M. 2012. The ubiquitin code. *Annu Rev Biochem* **81**:203–229. doi:10.1146/annurev-biochem-060310-170328

40. Kubori T, Shinzawa N, Kanuka H, Nagai H. 2010. *Legionella* metaeffector exploits host proteasome to temporally regulate cognate effector. *PLoS Pathog* **6**:e1001216. doi:10.1371/journal.ppat.1001216

41. Kubori T, Kitao T, Nagai H. 2019. Emerging insights into bacterial deubiquitinases. *Curr Opin Microbiol* **47**:14–19. doi:10.1016/j.mib.2018.10.001

42. Kunz TC, Götz R, Sauer M, Rudel T. 2019. Detection of *Chlamydia* developmental forms and secreted effectors by expansion microscopy. *Front Cell Infect Microbiol* **9**:276. doi:10.3389/fcimb.2019.00276

43. Lee JK, Enciso GA, Boassa D, Chander CN, Lou TH, Pairawan SS, Guo MC, Wan FYM, Ellisman MH, Sütterlin C, Tan M. 2018. Replication-dependent size reduction precedes differentiation in *Chlamydia trachomatis*. *Nat Commun* **9**:45. doi:10.1038/s41467-017-02432-0

44. Li J, Chai Q-Y, Liu CH. 2016. The ubiquitin system: a critical regulator of innate immunity and pathogen-host interactions. *Cell Mol Immunol* **13**:560–576. doi:10.1038/cmi.2016.40

45. Li Z, Chen C, Chen D, Wu Y, Zhong Y, Zhong G. 2008. Characterization of fifty putative inclusion membrane proteins encoded in the *Chlamydia trachomatis* genome. *Infect Immun* **76**:2746–2757. doi:10.1128/IAI.00010-08

46. Lowden NM, Yeruva L, Johnson CM, Bowlin AK, Fisher DJ. 2015. Use of aminoglycoside 3' adenyltransferase as a selection marker for *Chlamydia trachomatis* intron-mutagenesis and in vivo intron stability. *BMC Res Notes* **8**:570. doi:10.1186/s13104-015-1542-9

47. Lutter EI, Martens C, Hackstadt T. 2012. Evolution and conservation of predicted inclusion membrane proteins in *Chlamydiae*. *Comp Funct Genomics* **2012**:362104. doi:10.1155/2012/362104

48. Lutter EI, Barger AC, Nair V, Hackstadt T. 2013. *Chlamydia trachomatis* inclusion membrane protein CT228 recruits elements of the myosin phosphatase pathway to regulate release mechanisms. *Cell Rep* **3**:1921–1931. doi:10.1016/j.celrep.2013.04.027

49. Makarova KS, Aravind L, Koonin EV. 2000. A novel superfamily of predicted cysteine proteases from eukaryotes, viruses and *Chlamydia pneumoniae*. *Trends Biochem Sci* **25**:50–52. doi:10.1016/s0968-0004(99)01530-3

50. Meier K, Jachmann LH, Pérez L, Kepp O, Valdivia RH, Kroemer G, Sixt BS. 2022. The *Chlamydia* protein CpoS modulates the inclusion microenvironment and restricts the interferon response by acting on Rab35. *BioRxiv*. doi:10.1101/2022.02.18.481055

51. Misaghi S, Balsara ZR, Catic A, Spooner E, Ploegh HL, Starnbach MN. 2006. *Chlamydia trachomatis*-derived deubiquitinating enzymes in mammalian cells during infection. *Mol Microbiol* **61**:142–150. doi:10.1111/j.1365-2958.2006.05199.x

52. Mittal R, Peak-Chew S-Y, McMahon HT. 2006. Acetylation of MEK2 and IκB kinase (IKK) activation loop residues by YopJ inhibits signaling. *Proc Natl Acad Sci USA* **103**:18574–18579. doi:10.1073/pnas.0608995103

53. Mital J, Miller NJ, Fischer ER, Hackstadt T. 2010. Specific chlamydial inclusion membrane proteins associate with active Src family kinases in microdomains that interact with the host microtubule network. *Cell Microbiol***12**:1235–1249. doi:10.1111/j.1462-5822.2010.01465.x

54. Mizuno E, Kitamura N, Komada M. 2007. 14-3-3-dependent inhibition of the deubiquitinating activity of UBPY and its cancellation in the M phase. *Exp Cell Res* **313**:3624–3634. doi:10.1016/j.yexcr.2007.07.028

55. Moulder JW. 1991. Interaction of *Chlamydiae* and host cells in vitro. *Microbiol Rev* **55**:143–190.

56. Mukherjee S, Keitany G, Li Y, Wang Y, Ball HL, Goldsmith EJ, Orth K. 2006. *Yersinia* YopJ acetylates and inhibits kinase activation by blocking phosphorylation. *Science* **312**:1211–1214. doi:10.1126/science.1126867

57. Neunuebel MR, Chen Y, Gaspar AH, Backlund PS, Yergey A, Machner MP. 2011. De-AMPylation of the small GTPase Rab1 by the pathogen *Legionella pneumophila*. *Science* **333**:453–456. doi:10.1126/science.1207193

58. Nguyen BD, Valdivia RH. 2012. Virulence determinants in the obligate intracellular pathogen *Chlamydia trachomatis* revealed by forward genetic approaches. *Proc Natl Acad Sci USA* **109**:1263–1268. doi:10.1073/pnas.1117884109

59. Nguyen PH, Lutter EI, Hackstadt T. 2018. *Chlamydia trachomatis* inclusion membrane protein MrcA interacts with the inositol 1,4,5-trisphosphate receptor type 3 (ITPR3) to regulate extrusion formation. *PLoS Pathog***14**:e1006911. doi:10.1371/journal.ppat.1006911

60. Ohtake F, Tsuchiya H. 2017. The emerging complexity of ubiquitin architecture. *J Biochem* **161**:125–133. doi:10.1093/jb/mvw088

61. Pannekoek Y, Spaargaren J, Langerak AAJ, Merks J, Morré SA, van der Ende A. 2005. Interrelationship between polymorphisms of *incA*, fusogenic properties of *Chlamydia trachomatis* strains, and clinical manifestations in patients in The Netherlands. *J Clin Microbiol* **43**:2441–2443. doi:10.1128/JCM.43.5.2441-2443.2005

62. Peng J, Schwartz D, Elias JE, Thoreen CC, Cheng D, Marsischky G, Roelofs J, Finley D, Gygi SP. 2003. A proteomics approach to understanding protein ubiquitination. *Nat Biotechnol* **21**:921–926. doi:10.1038/nbt849

63. Pruneda JN, Durkin CH, Geurink PP, Ovaa H, Santhanam B, Holden DW, Komander D. 2016. The Molecular Basis for Ubiquitin and Ubiquitin-like Specificities in Bacterial Effector Proteases. *Mol Cell* **63**:261–276. doi:10.1016/j.molcel.2016.06.015

64. Pruneda JN, Bastidas RJ, Bertsoulaki E, Swatek KN, Santhanam B, Clague MJ, Valdivia RH, Urbé S, Komander D. 2018. A *Chlamydia* effector combining deubiquitination and acetylation activities induces Golgi fragmentation. *Nat Microbiol* **3**:1377–1384. doi:10.1038/s41564-018-0271-y

65. Reiley W, Zhang M, Wu X, Granger E, Sun S-C. 2005. Regulation of the deubiquitinating enzyme CYLD by IκB kinase gamma-dependent phosphorylation. *Mol Cell Biol* **25**:3886–3895. doi:10.1128/MCB.25.10.3886-3895.2005

66. Roan NR, Gierahn TM, Higgins DE, Starnbach MN. 2006. Monitoring the T cell response to genital tract infection. *Proc Natl Acad Sci USA* **103**:12069–12074. doi:10.1073/pnas.0603866103

67. Rockey DD, Scidmore MA, Bannantine JP, Brown WJ. 2002. Proteins in the chlamydial inclusion membrane. *Microbes Infect* **4**:333–340. doi:10.1016/s1286-4579(02)01546-0

68. Ronau JA, Beckmann JF, Hochstrasser M. 2016. Substrate specificity of the ubiquitin and Ubl proteases. *Cell Res* **26**:441–456. doi:10.1038/cr.2016.38

69. Rytkönen A, Poh J, Garmendia J, Boyle C, Thompson A, Liu M, Freemont P, Hinton JCD, Holden DW. 2007. SseL, a *Salmonella* deubiquitinase required for macrophage killing and virulence. *Proc Natl Acad Sci USA***104**:3502–3507. doi:10.1073/pnas.0610095104

70. Saeki Y. 2017. Ubiquitin recognition by the proteasome. *J Biochem* **161**:113–124. doi:10.1093/jb/mvw091

71. Schneider CA, Rasband WS, Eliceiri KW. 2012. NIH Image to ImageJ: 25 years of image analysis. *Nat Methods* **9**:671–675. doi:10.1038/nmeth.2089

72. Schubert AF, Nguyen JV, Franklin TG, Geurink PP, Roberts CG, Sanderson DJ, Miller LN, Ovaa H, Hofmann K, Pruneda JN, Komander D. 2020. Identification and characterization of diverse OTU deubiquitinases in bacteria. *EMBO J* **39**:e105127. doi:10.15252/embj.2020105127

73. Shaw JH, Key CE, Snider TA, Sah P, Shaw EI, Fisher DJ, Lutter EI. 2018. Genetic Inactivation of *Chlamydia trachomatis* Inclusion Membrane Protein CT228 Alters MYPT1 Recruitment, Extrusion Production, and Longevity of Infection. *Front Cell Infect Microbiol* **8**:415. doi:10.3389/fcimb.2018.00415

74. Sheedlo MJ, Qiu J, Tan Y, Paul LN, Luo Z-Q, Das C. 2015. Structural basis of substrate recognition by a bacterial deubiquitinase important for dynamics of phagosome ubiquitination. *Proc Natl Acad Sci USA* **112**:15090–15095. doi:10.1073/pnas.1514568112

75. Sixt BS, Bastidas RJ, Finethy R, Baxter RM, Carpenter VK, Kroemer G, Coers J, Valdivia RH. 2017. The *Chlamydia trachomatis* Inclusion Membrane Protein CpoS Counteracts STING-Mediated Cellular Surveillance and Suicide Programs. *Cell Host Microbe* **21**:113–121. doi:10.1016/j.chom.2016.12.002

76. Smith EP, Cotto-Rosario A, Borghesan E, Held K, Miller CN, Celli J. 2020. Epistatic Interplay between Type IV Secretion Effectors Engages the Small GTPase Rab2 in the *Brucella* Intracellular Cycle. *MBio* **11**. doi:10.1128/mBio.03350-19

77. Suchland RJ, Rockey DD, Bannantine JP, Stamm WE. 2000. Isolates of *Chlamydia trachomatis* that occupy nonfusogenic inclusions lack IncA, a protein localized to the inclusion membrane. *Infect Immun* **68**:360–367. doi:10.1128/IAI.68.1.360-367.2000

78. Swatek KN, Komander D. 2016. Ubiquitin modifications. *Cell Res* **26**:399–422. doi:10.1038/cr.2016.39

79. Tenno T, Fujiwara K, Tochio H, Iwai K, Morita EH, Hayashi H, Murata S, Hiroaki H, Sato M, Tanaka K, Shirakawa M. 2004. Structural basis for distinct roles of Lys63- and Lys48-linked polyubiquitin chains. *Genes Cells***9**:865–875. doi:10.1111/j.1365-2443.2004.00780.x

80. Urbanus ML, Quaile AT, Stogios PJ, Morar M, Rao C, Di Leo R, Evdokimova E, Lam M, Oatway C, Cuff ME, Osipiuk J, Michalska K, Nocek BP, Taipale M, Savchenko A, Ensminger AW. 2016. Diverse mechanisms of metaeffector activity in an intracellular bacterial pathogen, *Legionella pneumophila*. *Mol Syst Biol* **12**:893. doi:10.15252/msb.20167381

81. Varadan R, Walker O, Pickart C, Fushman D. 2002. Structural properties of polyubiquitin chains in solution. *J Mol Biol* **324**:637–647. doi:10.1016/s0022-2836(02)01198-1

82. Vozandychova V, Stojkova P, Hercik K, Rehulka P, Stulik J. 2021. The Ubiquitination System within Bacterial Host-Pathogen Interactions. *Microorganisms* **9**. doi:10.3390/microorganisms9030638

83. Wang X, Hybiske K, Stephens RS. 2018. Direct visualization of the expression and localization of chlamydial effector proteins within infected host cells. *Pathog Dis* **76**. doi:10.1093/femspd/fty011

84. Weber MM, Bauler LD, Lam J, Hackstadt T. 2015. Expression and localization of predicted inclusion membrane proteins in *Chlamydia trachomatis*. *Infect Immun* **83**:4710–4718. doi:10.1128/IAI.01075-15

85. Weeks SD, Grasty KC, Hernandez-Cuebas L, Loll PJ. 2009. Crystal structures of Lys-63-linked tri- and di-ubiquitin reveal a highly extended chain architecture. *Proteins* **77**:753–759. doi:10.1002/prot.22568

86. Wesolowski J, Weber MM, Nawrotek A, Dooley CA, Calderon M, St Croix CM, Hackstadt T, Cherfils J, Paumet F. 2017. *Chlamydia* hijacks ARF gtpases to coordinate microtubule posttranslational modifications and golgi complex positioning. *MBio* **8**. doi:10.1128/mBio.02280-16

87. Zadora PK, Chumduri C, Imami K, Berger H, Mi Y, Selbach M, Meyer TF, Gurumurthy RK. 2019. Integrated Phosphoproteome and Transcriptome Analysis Reveals *Chlamydia*-Induced Epithelial-to-Mesenchymal Transition in Host Cells. *Cell Rep* **26**:1286-1302.e8. doi:10.1016/j.celrep.2019.01.006

88. Zhou Y, Zhou B, Pache L, Chang M, Khodabakhshi AH, Tanaseichuk O, Benner C, Chanda SK. 2019. Metascape provides a biologist-oriented resource for the analysis of systems-level datasets. *Nat Commun* **10**:1523. doi:10.1038/s41467-019-09234-6

89. Zuck M, Ellis T, Venida A, Hybiske K. 2017. Extrusions are phagocytosed and promote *Chlamydia* survival within macrophages. *Cell Microbiol* **19**. doi:10.1111/cmi.12683

90. Zuck M, Sherrid A, Suchland R, Ellis T, Hybiske K. 2016. Conservation of extrusion as an exit mechanism for *Chlamydia*. *Pathog Dis* **74**. doi:10.1093/femspd/ftw093

Figures

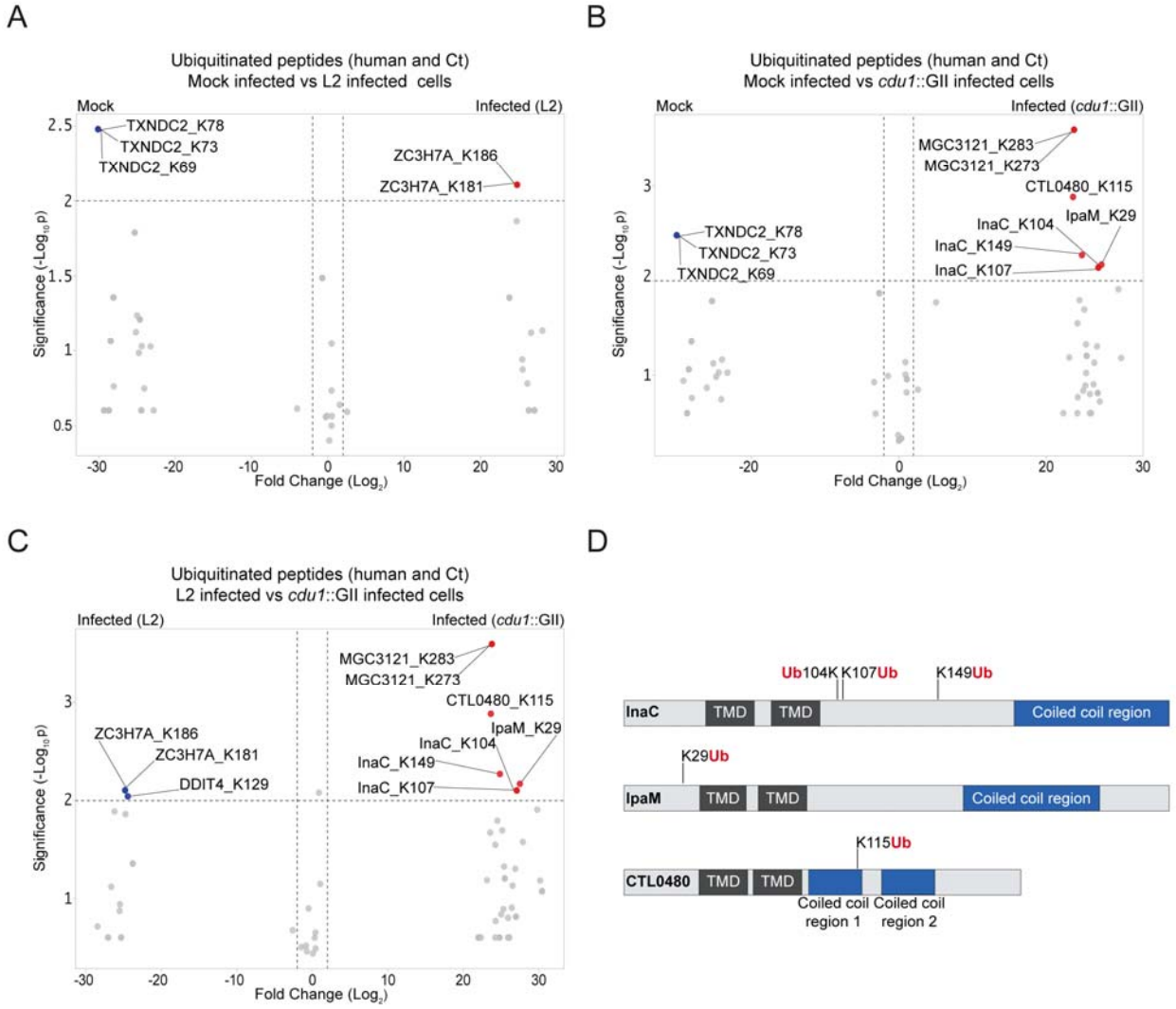

Figure 1

The *C. trachomatis* inclusion membrane proteins InaC, IpaM, and CTL0480 are ubiquitinated in the absence of Cdu1. (A-C) Volcano plots (pairwise comparisons) of the relative abundance of human and Ct ubiquitinated peptides between mock infected HeLa cells versus HeLa cells infected with L2 (24 hpi) **(A),** mock infected HeLa cells versus HeLa cells infected with a *cdu1* null strain (*cdu1*::GII) (24 hpi) **(B),** and HeLa cells infected with L2 (24 hpi) versus HeLa cells infected with a *cdu1* null strain (24 hpi) **(C)**. All infections were performed for 24 hours. Significance values were interpolated from 3 independent biological replicates. Ubiquitinated proteins were enriched with magnetic TUBE 1 beads (binds to polyubiquitinated proteins) and peptides identified by quantitative LC MS/MS analysis. Three Ct proteins, InaC, IpaM, and CTL0480 were differentially ubiquitinated in the absence of Cdu1. **(D)** InaC was ubiquitinated at K104, K107, and K149, IpaM at K290, and CTL0480 at K115 in the absence of Cdu1. TMD: Transmembrane domain. Numbering corresponds to amino acids in the protein sequence of each respective inclusion membrane protein.

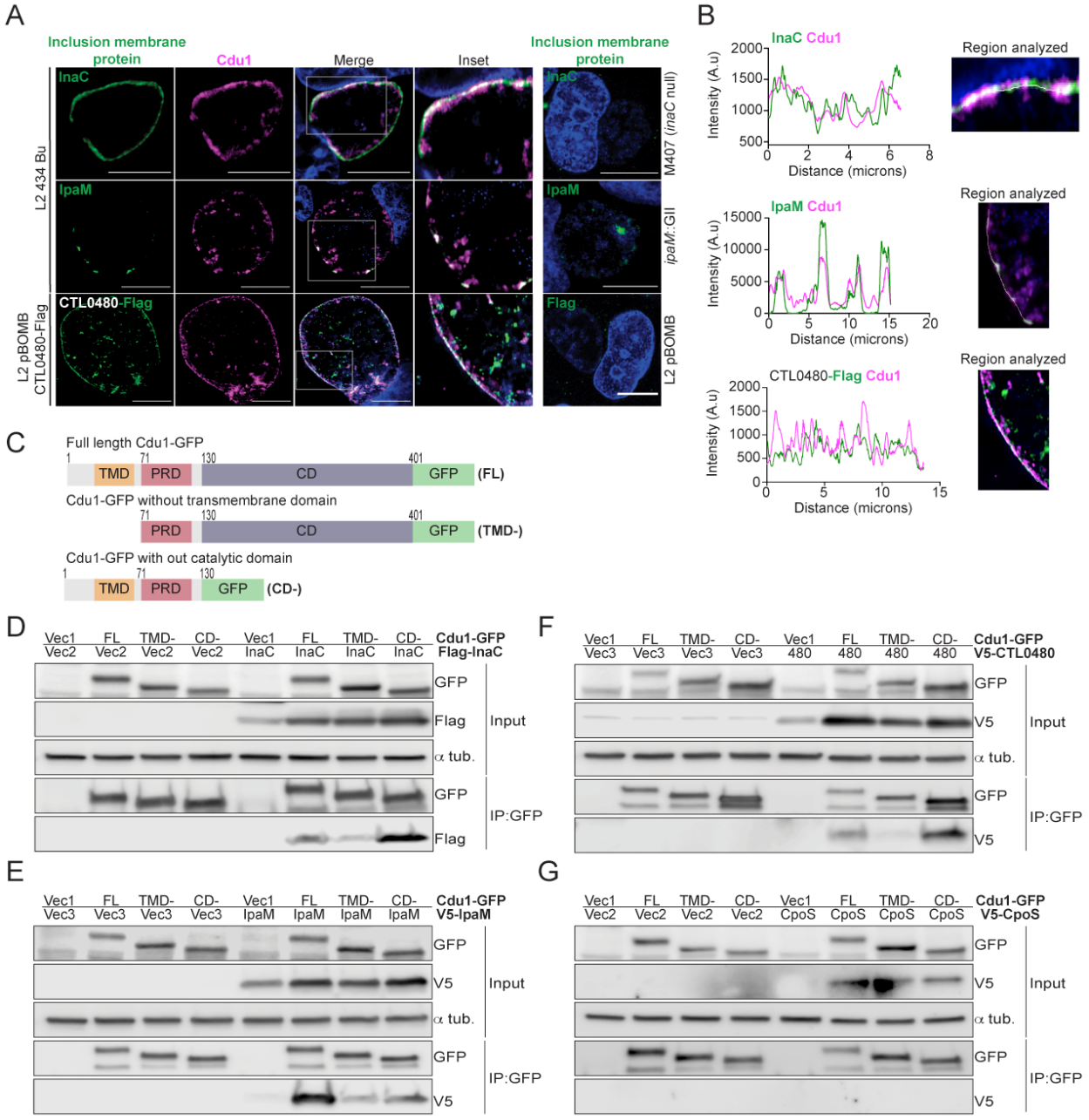

Figure 2

Cdu1 associates with InaC, IpaM, and CTL0480. (A) Co-localization of Cdu1(magenta) with endogenous InaC (green), IpaM (green), and ectopically expressed CTL0480-Flag (green) at the L2 inclusion membrane during infection of HeLa cells at 24 hpi. HeLa cells infected with an *inaC* null strain (M407), an *ipaM* null strain (*ipaM*::GII), and L2 pBOMB were used as antibody specificity controls. DNA stained with Hoechst is shown in blue. Scale bar: 10µm. Images are representative of multiple images captured across three independent replicates. **(B)** Line scan profiles of fluorescent signal intensities displayed in (A) showing co-localization of fluorescence intensities for endogenous Cdu1 with endogenous InaC, and IpaM and with CTL0480-Flag

along the L2 inclusion membrane. **(C)** Schematic of Cdu1-GFP(C) (L2) fusion (Cdu1-GFP) and Cdu1-GFP variants used in co-transfections of HEK 293 cells. GFP: Green fluorescent protein. TMD: Transmembrane domain. PRD: Proline rich domain. CD: Catalytic domain. FL: Full length. TMD-: Cdu1-GFP variant lacking TMD domain. CD-: Cdu1-GFP variant lacking CD domain. **(D-G)** Western blot analysis of GFP immunoprecipitates from HEK 293 cells co-transfected with mammalian plasmids expressing: Cdu1-GFP variants and **(D)** truncated 3XFlag(N)-InaC (D/UW-3/CX CT813, amino acids 96-264), **(E)** V5(N)-IpaM (L2, full length), **(F)** V5(N)-CTL0480 (L2, full length), and **(G)** V5(N)-CpoS (L2, full length). Vec1: Empty pOPINN-GFP vector. Vec2: Empty pDEST53 vector. Vec3: Empty pcDNA^{TM}3.1/nV5-DEST vector. Western blot images are representative from two independent experiments.

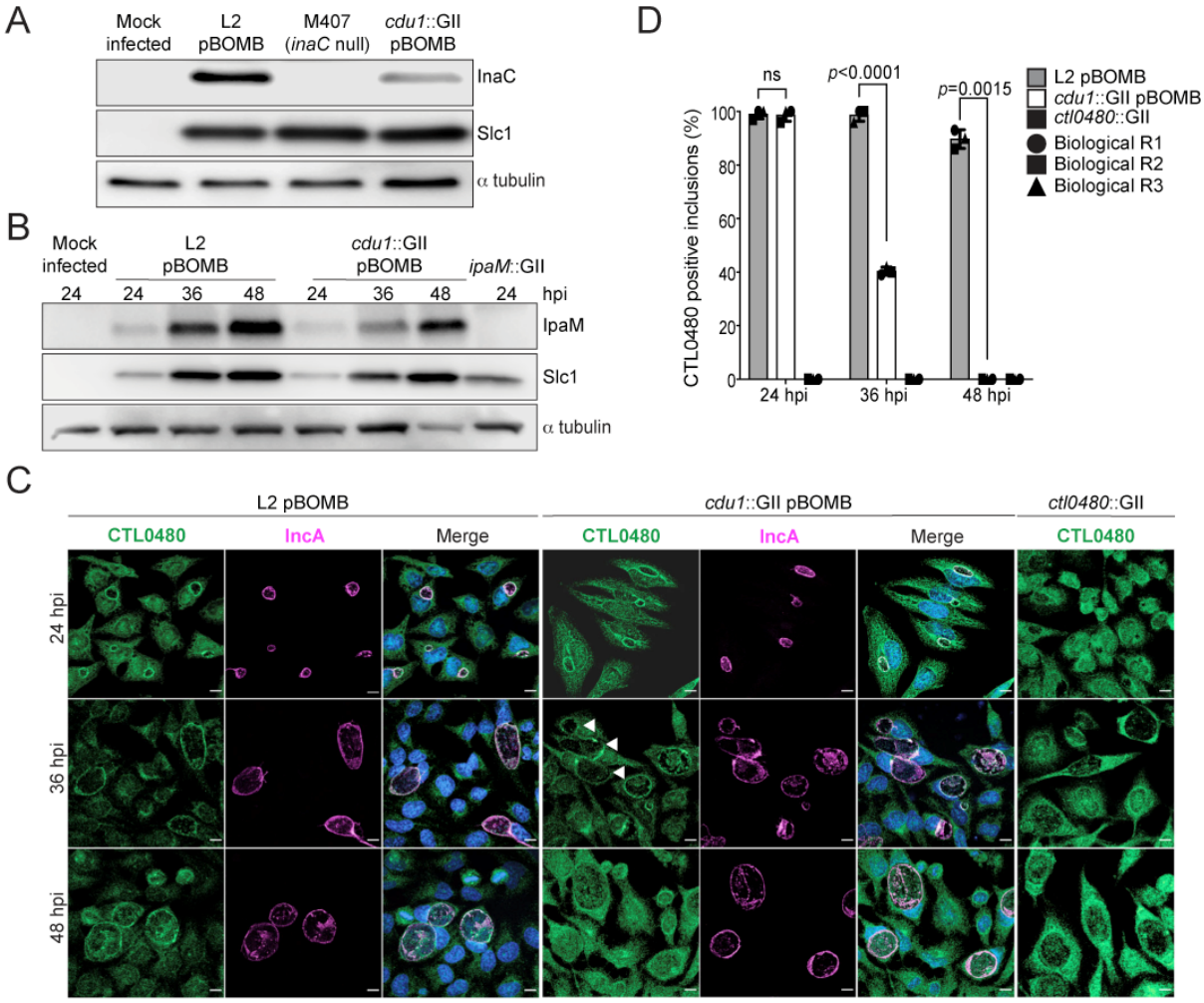

Figure 3

Cdu1 stabilizes InaC, IpaM, and CTL0480. (A) Western blot analysis of InaC in HeLa cells infected for 24 hours with L2, *inaC* null, and *cdu1* null strains. Ct Slc1 and human alpha tubulin were used to determine Ct burdens and equal loading of protein extracts respectively. Western blot images are representative of 3 independent experiments. **(B)** Western blot analysis of endogenous IpaM in HeLa cells infected with L2, *cdu1* null, and *ipaM* null strains for 24, 36, and 48 hours. Western blot images are representative of 2 independent experiments. **(C)** Localization of CTL0480 during Ct infection of HeLa cells at 24, 36, and 48 hpi. CTL0480 signal (green) co-localizes with the inclusion membrane protein IncA (magenta) at the L2 inclusion membrane. Arrowheads highlight *cdu1* null inclusions lacking CTL0480 at 36 hpi. DNA stained with Hoechst is shown in blue. Scale bar: 10µm. **(D)** Quantification of CTL0480 localization at Ct inclusion membranes as shown in (C). CTL0480 fluorescent signal was used to determine the percent of inclusions displaying CTL0480 at the inclusion membranes. Representative images and quantification of CTL0480 positive inclusions are derived from Ct inclusions imaged in 10 fields across 3 independent biological replicates. *p* values were determined by a student paired t-test.

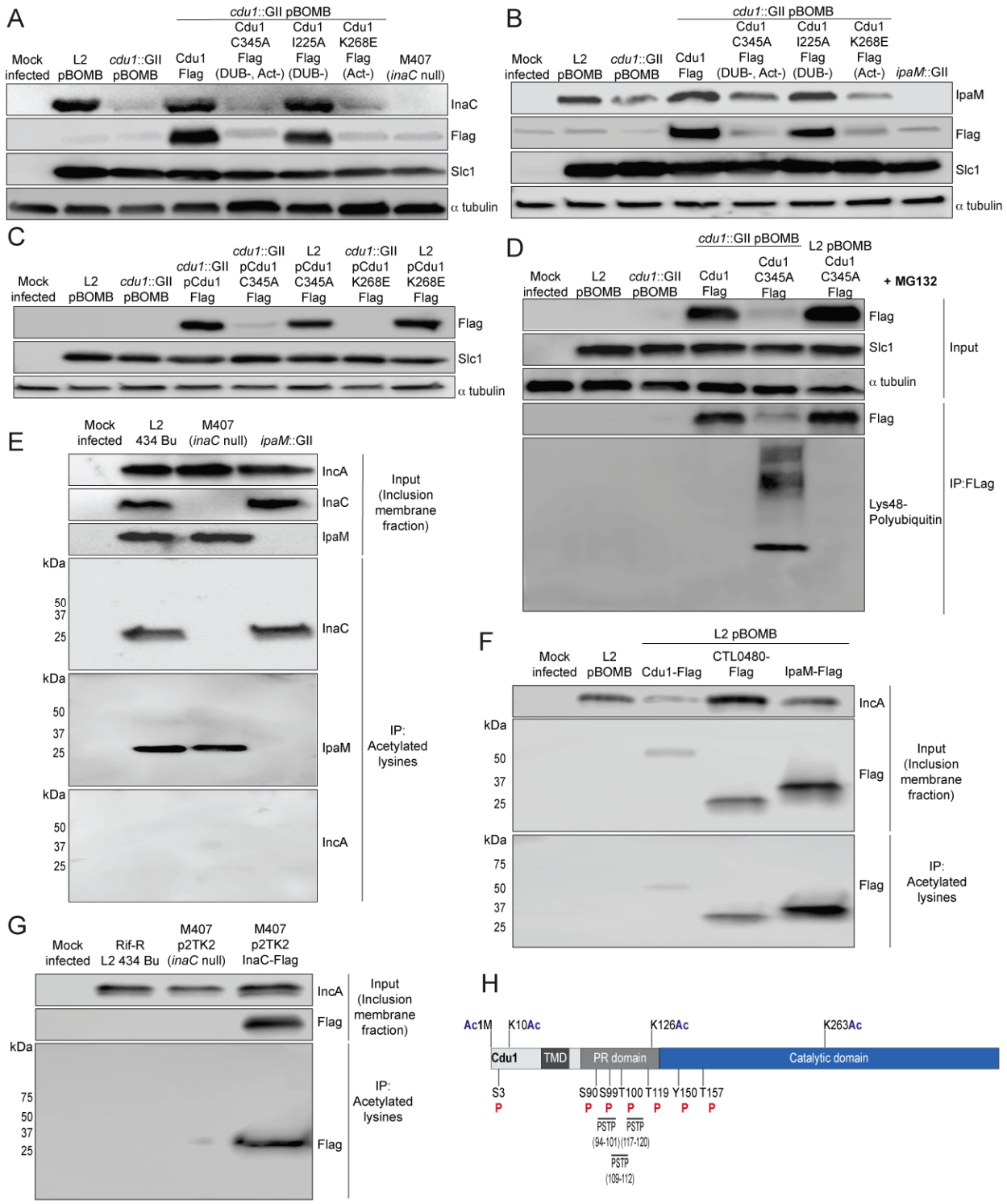

Figure 4

The acetylase activity of Cdu1 is required to stabilize Cdu1, InaC, and IpaM. (A) Western blot analysis of endogenous InaC and Cdu1-Flag catalytic variants expressed from a plasmid. HeLa cells were infected for 36 hours with L2, a *cdu1* null strain, and *cdu1* null strains expressing wild type Cdu1-Flag and the Cdu1 variants C345A-Flag (catalytic inactive), I225A-

Flag (DUB deficient), and K268E-Flag (Act deficient). Protein lysates from HeLa cells infected with M407 (*inaC* null) were used to control for the specificity of anti-InaC antibodies. Western blot images are representative of two independent experiments. **(B)** Western blot analysis of endogenous IpaM and Cdu1-FLAG variants in crude extracts of HeLa cells infected for 48 hours with the same strains as describe in (A). Infection of HeLa cells with *ipaM*::GII was used to test for the specificity of the anti-IpaM antibody. Western blot images are representative of two independent experiments. **(C)** Western blot analysis of Cdu1^{C345A}-Flag (catalytic inactive) and Cdu1^{K268E}-Flag (Act deficient) expressed in a *cdu1* null strain or wild type L2 background after infection of HeLa cells for 24 hours. Both Cdu1 variants are stabilized by endogenous Cdu1. **(D)** Western blot analysis of Cdu1-Flag and Cdu1^{C345A}-Flag expressed in a *cdu1* null strain and Cdu1^{C345A}-Flag expressed in wild type L2 following immunoprecipitation (anti-Flag) from HeLa cell extracts after infection for 24 hours and treatment with MG132 (25 μM, 5 hours). Western blot image is a representative blot from at least three independent experiments. **(E)** Western blot analysis of endogenous InaC and IpaM following immunoprecipitation of proteins acetylated at lysines from inclusion membrane subcellular fractions derived from HeLa cells infected with WT L2 for 24 hours. Western blot image is representative of two independent experiments. **(F)** Western blot analysis (Flag WB) of acetylated lysine immunoprecipitates generated from inclusion membrane subcellular fractions derived from HeLa cells infected with WT L2 strains expressing Cdu1-Flag, CTL0480-Flag, and IpaM-Flag at 40 hpi. Western blot image is representative of two independent experiments. **(G)** Flag WB of acetylated lysine immunoprecipitates generated from inclusion membrane subcellular fractions derived from HeLa cells infected with Rif-R L2 (M407 parental strain) and with M407 (*inaC* null) expressing InaC-Flag at 24 hpi. Western blot image is representative of two independent experiments. **(H)** The initiator methionine, Lys10, Lys126, and Lys263 of Cdu1 are acetylated during Ct infection of HeLa cells (24 hpi). One tyrosine (Y) residue and multiple serine (S) and threonine (T) residues in Cdu1 are also phosphorylated during Ct infection of HeLa cells (24 hpi). Three PX(S/T)P MAPK phosphorylation consensus sequence motifs were identified in the proline rich domain of Cdu1. Modified residues were identified by quantitative LC MS/MS analysis of immunoprecipitated Cdu1-Flag across 3 independent biological replicates. TMD: Transmembrane domain. PR: Proline rich. PSTP: PX(S/T)P motifs. Ac: Acetylation. P: Phosphorylation. Numbering corresponds to amino acids in Cdu1 protein sequence.

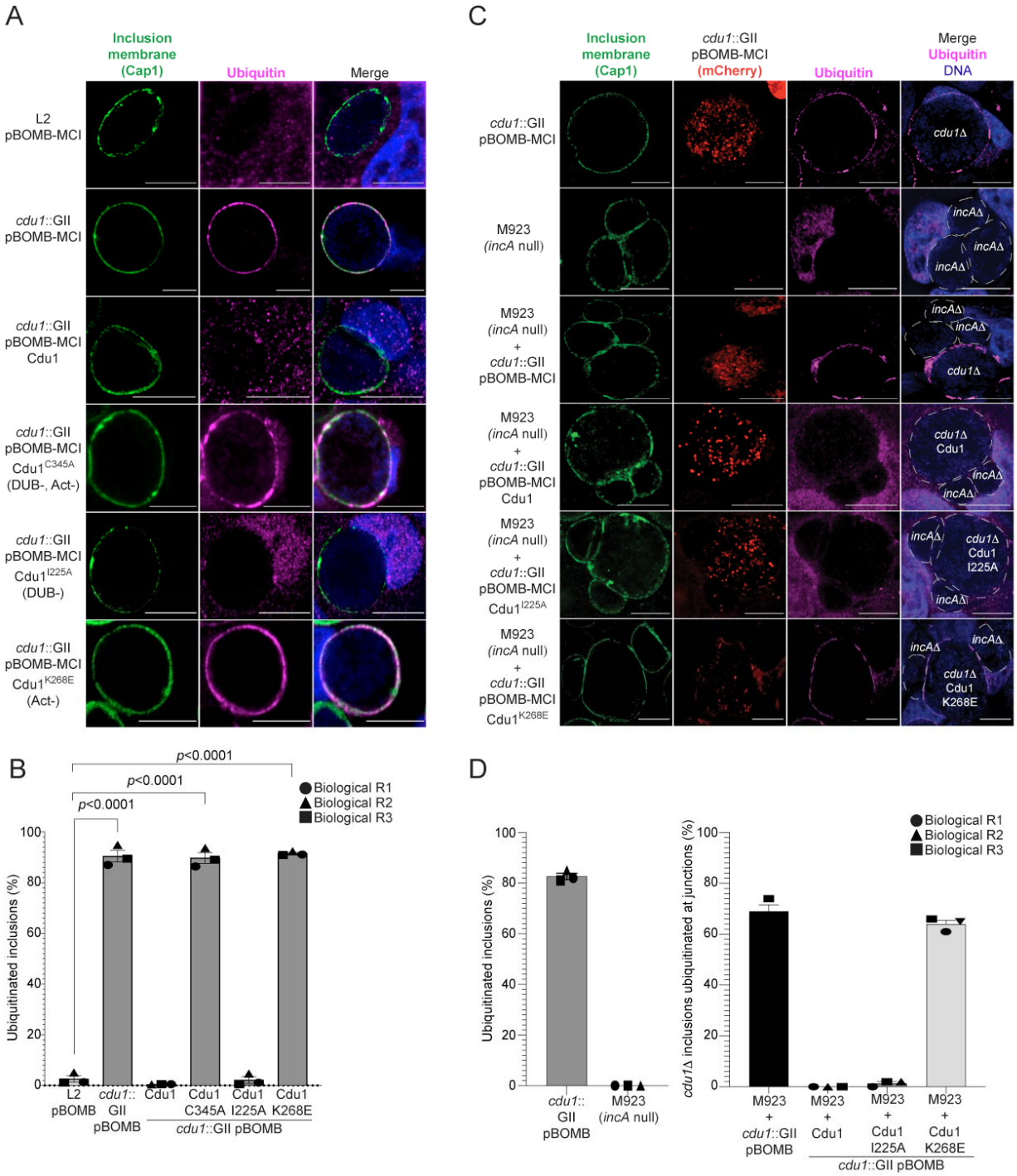

Figure 5

The DUB activity of Cdu1 is not required for blocking the ubiquitination of inclusion membranes. (A) Loss of Cdu1's acetylase activity results in the accumulation of Ub (magenta signal) at the periphery of the inclusion. HeLa cells were infected for 24 hours. Antisera against the membrane protein Cap1 (green) was used to mark inclusion membranes. DNA stained with Hoechst is shown in blue. Scale bar: 10µm. **(B)** Quantification of ubiquitinated inclusions as shown in (A). The Ub fluorescent signal was used to determine the number of infected cells with

Ub decorated inclusions. The total number of ubiquitinated inclusions was divided by the total number of inclusions analyzed (defined by Cap1 staining). 87%, 86%, and 91% of inclusions were decorated with Ub in HeLa cells infected with a *cdu1* null strain and *cdu1* null strains expressing Cdu1^{C345A} (DUB-, Act-), and Cdu1^{K268E} (Act-) variants respectively. Representative images in (A) and quantification of ubiquitinated inclusions in (B) were obtained from inclusions imaged in 10 fields across 3 independent biological replicates for each strain. *p* values were determined by a student paired t-test. **(C)** HeLa cells co-infected with *cdu1*::GII (*cdu1⊿*) and *incA* null (*incA*Δ, M923) strains at 24 hpi. IncA-deficient inclusions do not fuse with other inclusions. In co-infected cells, Cdu1 present on the inclusion membranes of *incA⊿* strains did not block ubiquitination events at or near the inclusion membranes of neighboring *cdu1⊿* strains (mCherry signal from pBOMB4-MCI plasmid). DNA stained with Hoechst is shown in blue. Scale bar: 10µm. **(D)** Quantification of *cdu1⊿* inclusions as shown in (C) in which ubiquitination events are observed in regions of *cdu1⊿* inclusion membranes that are in direct apposition to *incA⊿* inclusion membranes (junctions). The total number of *cdu1⊿* inclusions ubiquitinated at inclusion junctions was divided by the total number of inclusions analyzed (Cap1 staining). 66% and 61% of *cdu1⊿* inclusions were decorated with Ub at junctions in HeLa cells co-infected with *incA⊿* and *cdu1⊿* strains or with *incA⊿* and a *cdu1⊿* strain ectopically expressing Cdu1^{K268E} (Act-) respectively. Representative images in (C) and quantification of *cdu1⊿* inclusions ubiquitinated at junctions in (D) are derived from inclusions imaged in 6 fields across 3 independent biological replicates for each condition. *p* values were determined by a student paired t-test.

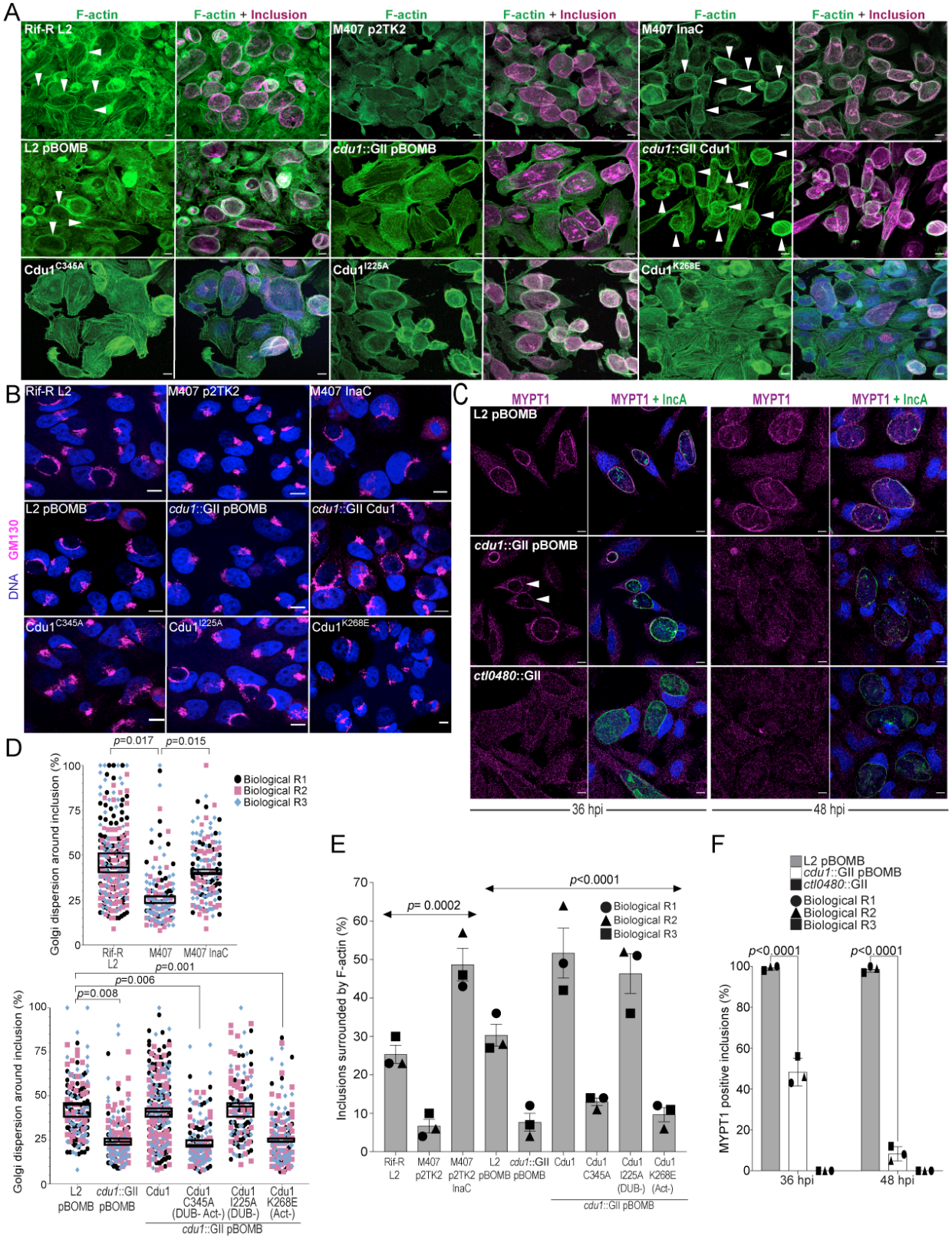
A
F-actin
F-actin + Inclusion
Rif-R L2
M407 p2TK2
M407 InaC
L2 pBOMB
cdu1::GII pBOMB
cdu1::GII Cdu1
Cdu1C345A
Cdu1I225A
Cdu1K268E
B
GM130
DNA
C
MYPT1
MYPT1 + IncA
ctl0480::GII
36 hpi
48 hpi
D
Golgi dispersion around inclusion (%)
Biological R1
Biological R2
Biological R3
p=0.017
p=0.015
p=0.008
p=0.006
p=0.001
E
Inclusions surrounded by F-actin (%)
p= 0.0002
p<0.0001
F
MYPT1 positive inclusions (%)
p<0.0001

Figure 6

The DUB activity of Cdu1 is not required for assembly of F-actin or Golgi ministack repositioning around the Ct inclusion while Cdu1 is required for MYPT1 recruitment to the inclusion.

Representative images of F-actin (green, Alexa Fluor™ Phalloidin) assembled around the Ct inclusion (magenta, anti Cdu1 and Cap1 staining) in HeLa cells infected for 40 hours. **(B)** Representative images of Golgi (anti GM130 staining, magenta) around Ct inclusions (arrowheads) in HeLa cells infected for 24 hours. HeLa cells were infected with an *inaC* null strain transformed with empty p2TK2 vector (M407 p2TK2), the wild type strain in which M407 was derived from (Rif-R L2) and M407 ectopically expressing full length InaC (M407 p2TK2-InaC). HeLa cells were also infected with L2 pBOMB, *cdu1*::GII pBOMB, and *cdu1* null strains ectopically expressing Cdu1-Flag (Cdu1), and the Cdu1 variants C345A-Flag (DUB-, Act-), I225A-Flag (DUB-), and K268E-Flag (Act-). **(C)** Representative images of MYPT1 (magenta) at Ct inclusions (green, anti-IncA staining). Arrowheads represent *cdu1* null inclusions with low MYPT1 signal. DNA stained with Hoechst is shown in blue in panels A-C. Scale bar: 10µm in panels A-C. **(D)** Quantification of Golgi dispersal around the Ct inclusion as shown in (B). The length of Golgi dispersed around each Ct inclusion imaged was measured and normalized to the perimeter length of each inclusion (% Golgi dispersion around the inclusion). Representative images in (B) and Golgi dispersal quantified in (D) were performed from inclusions imaged in 6 fields across 3 independent biological replicates. *p* values were determined by a student paired t-test. **(E)** Quantification of Ct inclusion surrounded by F-actin as shown in (A) normalized to total inclusions analyzed. Representative images in (A) and quantification of F-actin surrounding Ct inclusions in (E) were obtained from inclusions imaged in 6 fields across 3 independent biological replicates. *p* values were determined by one-way ANOVAs with a Student-Newman-Keuls post hoc test. **(F)** Quantification of MYPT1 at Ct inclusions as shown in (C). Representative images in (C) and quantification of MYPT1 recruitment in (F) were obtained from inclusions imaged in 6 fields across 3 independent replicates. *p* values were determined by a student paired t-test.

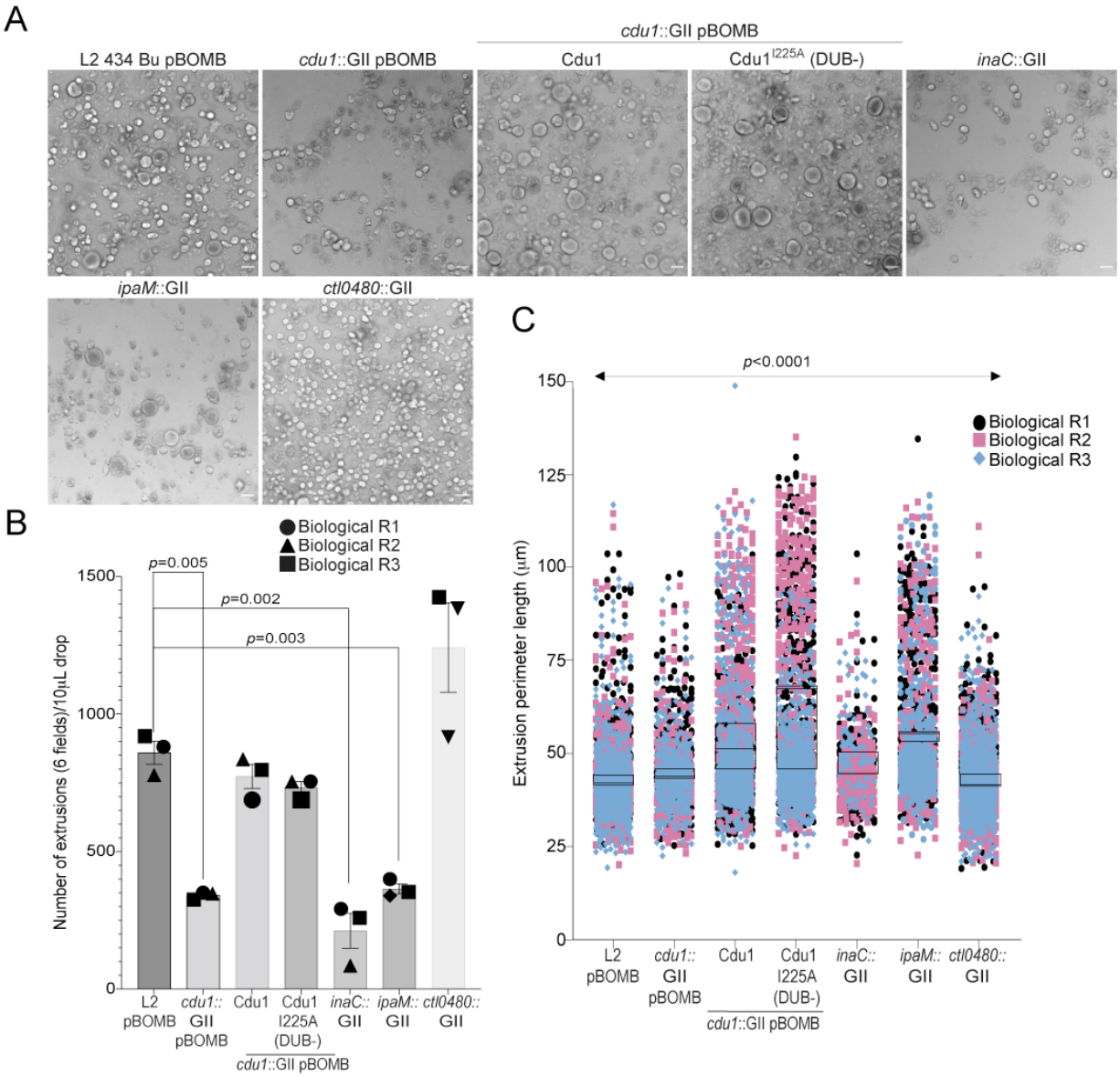

Figure 7

Cdu1, InaC, and IpaM are required for optimal extrusion of Ct inclusions from HeLa cells. **(A)** Representative images of extrusions isolated from HeLa cell monolayers infected with Ct strains for 52 hours. Scale bar: 200 µm **(B)** Quantification of the number of extruded inclusions produced by infected HeLa cell monolayers. *p* values were determined by a student paired t-test. **(C)** Quantification of the size of extruded inclusions quantified in (B). Extruded inclusions varied in size among cells infected with wild type L2 (average :43 µm), *ipaM* mutants (average: 56 µm) and *cdu1* mutants complemented wild type Cdu1 (average: 52 µm) and Cdu1^{I225A} (DUB-) (average: 60 µm). *p* values were determined by one-way ANOVAs with a Student-Newman-Keuls post hoc test. Representative images in (A) and quantification of extrusion number in (B) and extrusion size in (C) are based on images obtained from 6 fields across 3 independent biological replicates.

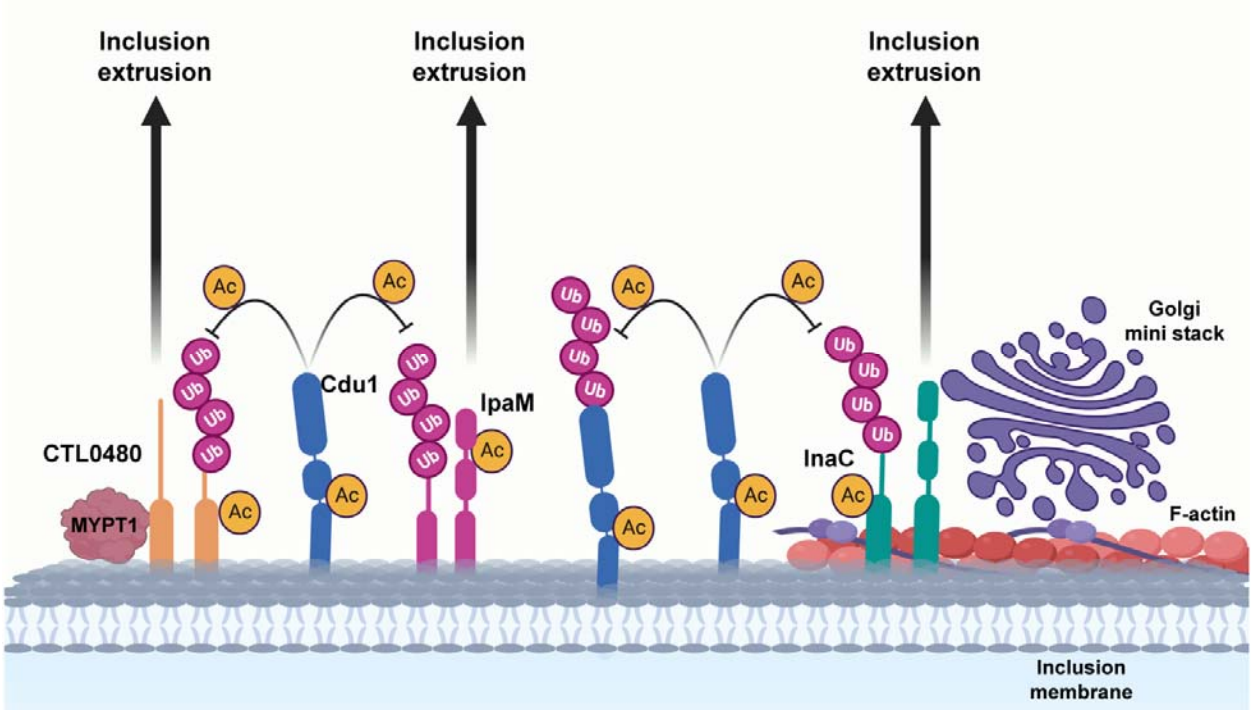

Figure 8.
A model for acetylation mediated protection of the translocated Ct effectors InaC, IpaM, and CTL0480 from degradation.
The human cellular Ub machinery targets *C. trachomatis* effectors, including the inclusion membrane proteins InaC, IpaM, and CTL0480 for ubiquitination and subsequent protein degradation. *C. trachomatis* has evolved strategies to counter such defense mechanisms by translocating the effector Cdu1. Cdu1 utilizes its acetylase activity rather than its deubiquitinase activity to protect itself and all three inclusion membrane proteins from being targeted for ubiquitination and degradation. Cdu1 protects InaC in order to promote the recruitment of F-actin scaffolds and Golgi ministacks to the inclusion perimeter and CTL0480 to recruit the Myosin II regulator MYPT1. All three inclusion proteins and Cdu1 also participate in promoting extrusion of *C. trachomatis* inclusions late in infection. Image created with BioRender.com.

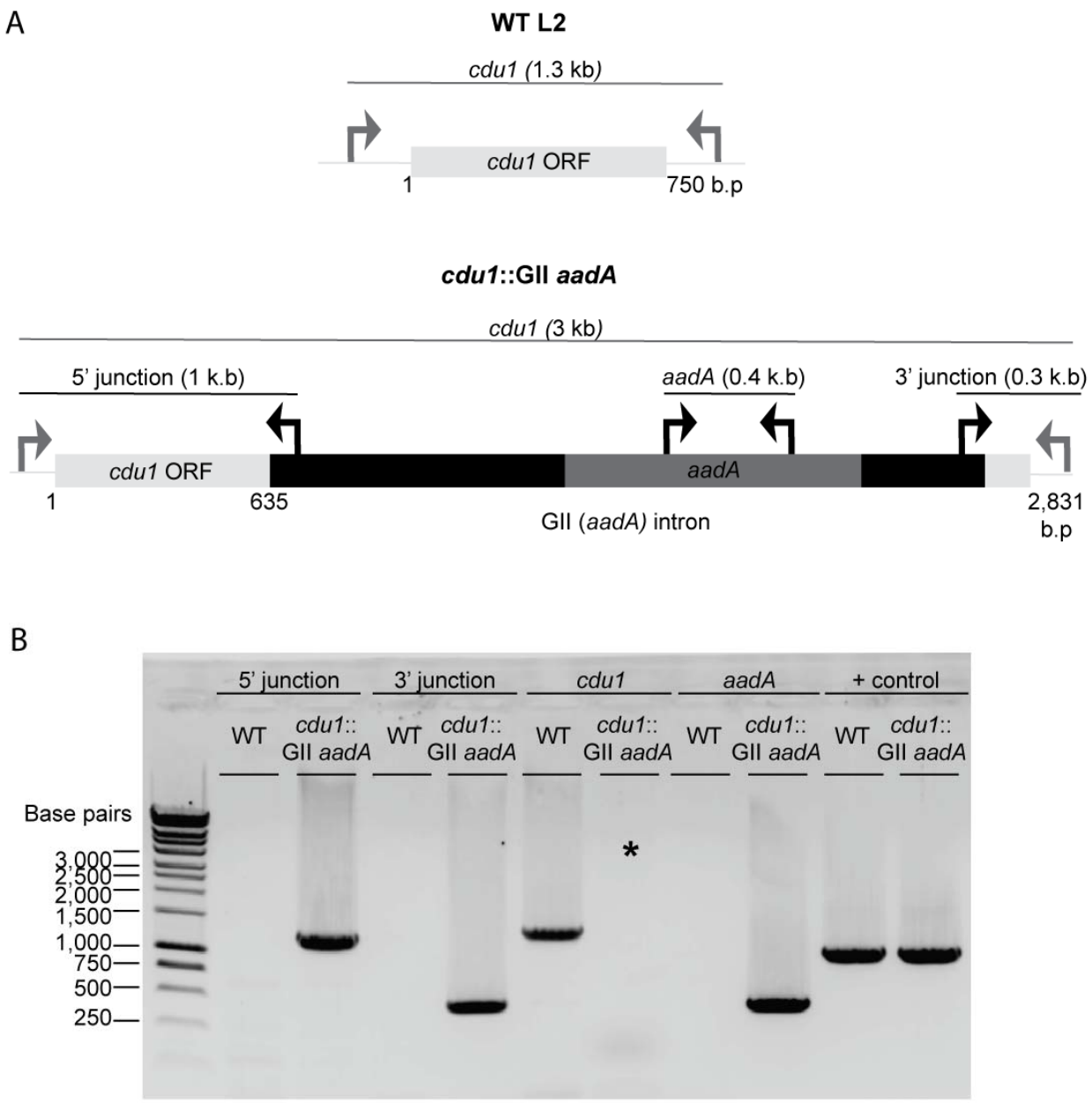

Supplementary Figure 1
TargeTron mediated disruption of the L2 *cdu1* ORF. (**A**) Depiction of the *cdu1* ORFs in WT L2 and *cdu1*::GII strains with corresponding diagnostic PCR amplicons. (**B**) PCR analysis of the disrupted *cdu1* ORF in the *cdu1*::GII strain. *Amplification of *cdu1* ORF in *cdu1*::GII strain was unsuccessful due to size of amplicon.

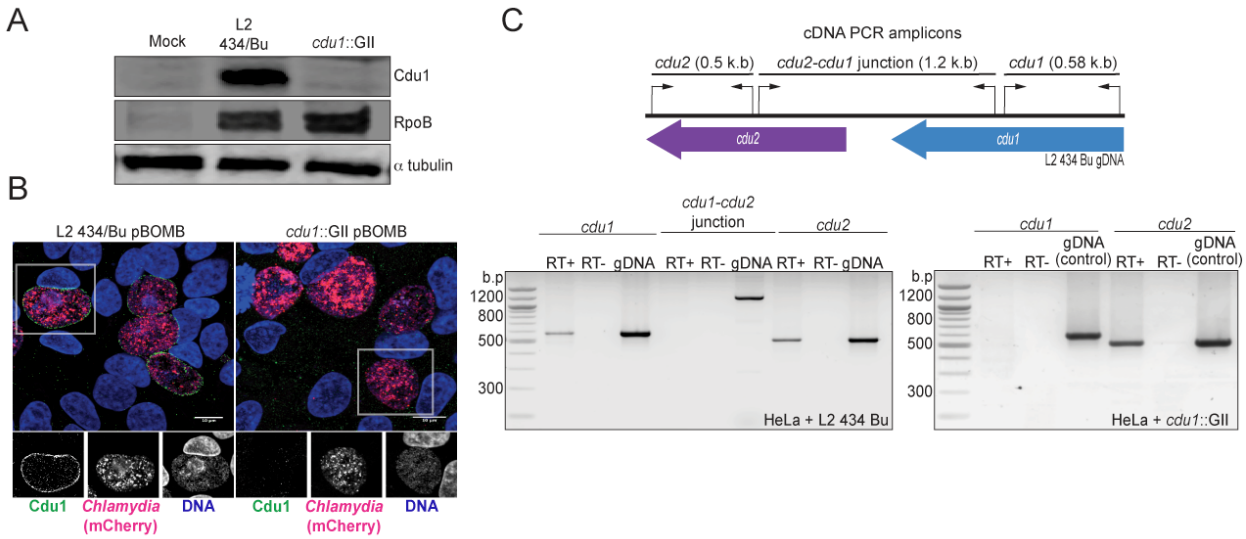

Supplementary Figure 2

Generation of a *cdu1* null strain in *C. trachomatis* (L2). (**A**) Western blot analysis of protein lysates derived from HeLa cells infected with a Ct L2 434 Bu parental strain (L2) and an L2 *cdu1*::GII *aadA* (*cdu1*::GII) strain for 24 hours. Blots were probed with antibodies raised against recombinant Cdu1 (amino acids 71-401), Ct RpoB (bacterial RNA polymerase), and human α tubulin. (**B**) HeLa cells infected with L2 transformed with pBOMB4-MCI empty vector (L2 pBOMB) and *cdu1*::GII transformed with empty pBOMB4-MCI (*cdu1*::GII pBOMB) were fixed at 24 hpi and stained with Cdu1 antisera. Cdu1 signal is depicted in green, Ct cells expressing mCherry (encoded in pBOMB4-MCI vector) are shown in red, and DNA stained with Hoechst in blue. Scale bar: 10µm. (**C**) Total RNA isolated from HeLa cells infected with L2 and *cdu1*::GII strains for 24 hours was used to synthesize cDNAs which served as templates for PCR analysis of *cdu1*, *cdu2*, and *cdu1-cdu2* bicistronic expression. RT+: Total RNA + reverse transcriptase. RT-: Total RNA without reverse transcriptase. gDNA: Genomic DNA.

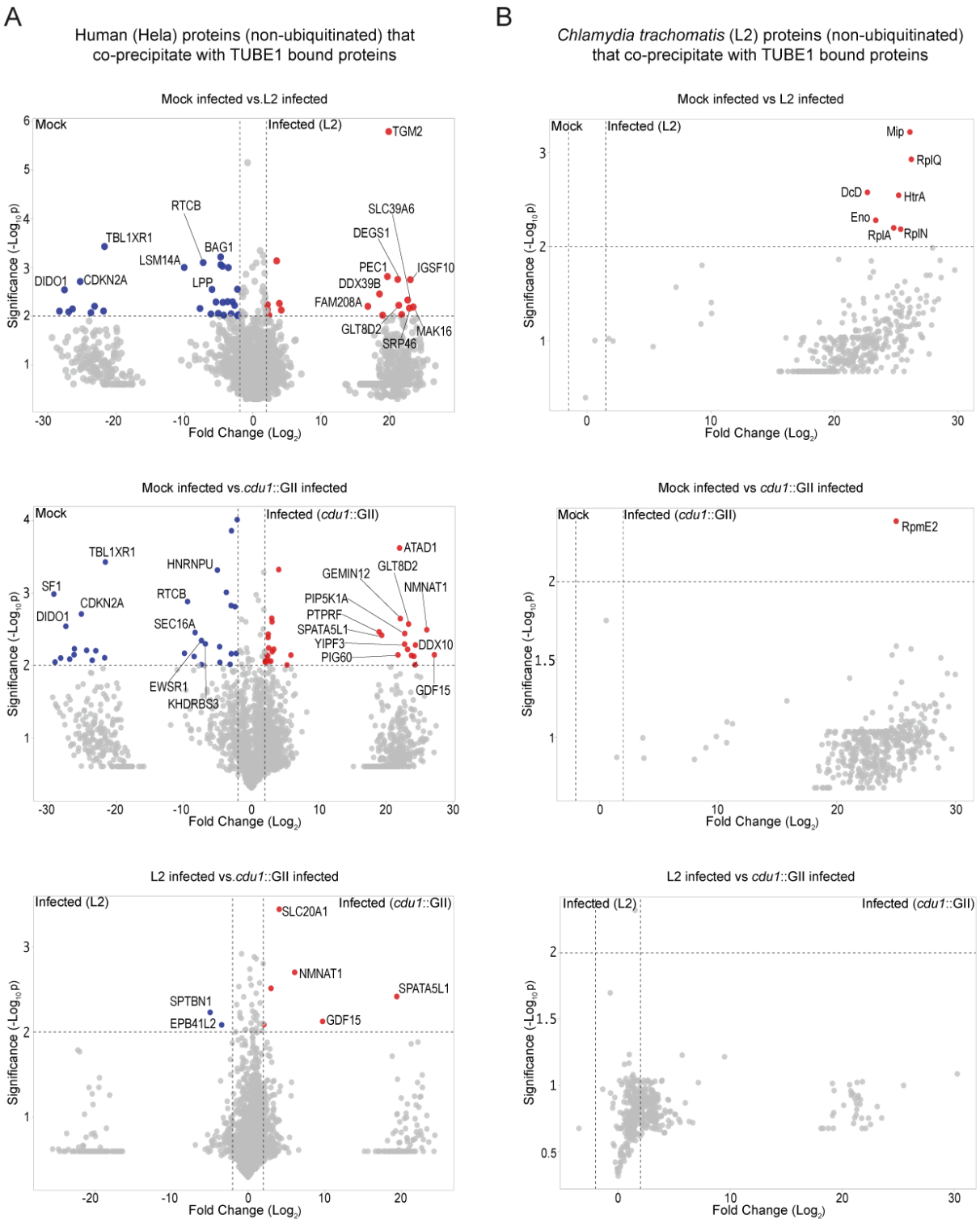

Supplementary Figure 3

Proteins co-precipitating (non ubiquitinated) with human and Ct proteins enriched by TUBE 1 pulldowns. (A) Volcano plots (pairwise comparisons) of human proteins (non-ubiquitinated) that co-precipitate with TUBE1 bound proteins in mock infected HeLa cells and HeLa cells infected with L2 or *cdu1* null strains (24 hpi). **(B)** Volcano plots (pairwise

comparisons) of Ct TUBE1 co-precipitating proteins (non-ubiquitinated) identified in mock infected HeLa cells and HeLa cells infected with L2 or *cdu1* null strains (24 hpi).

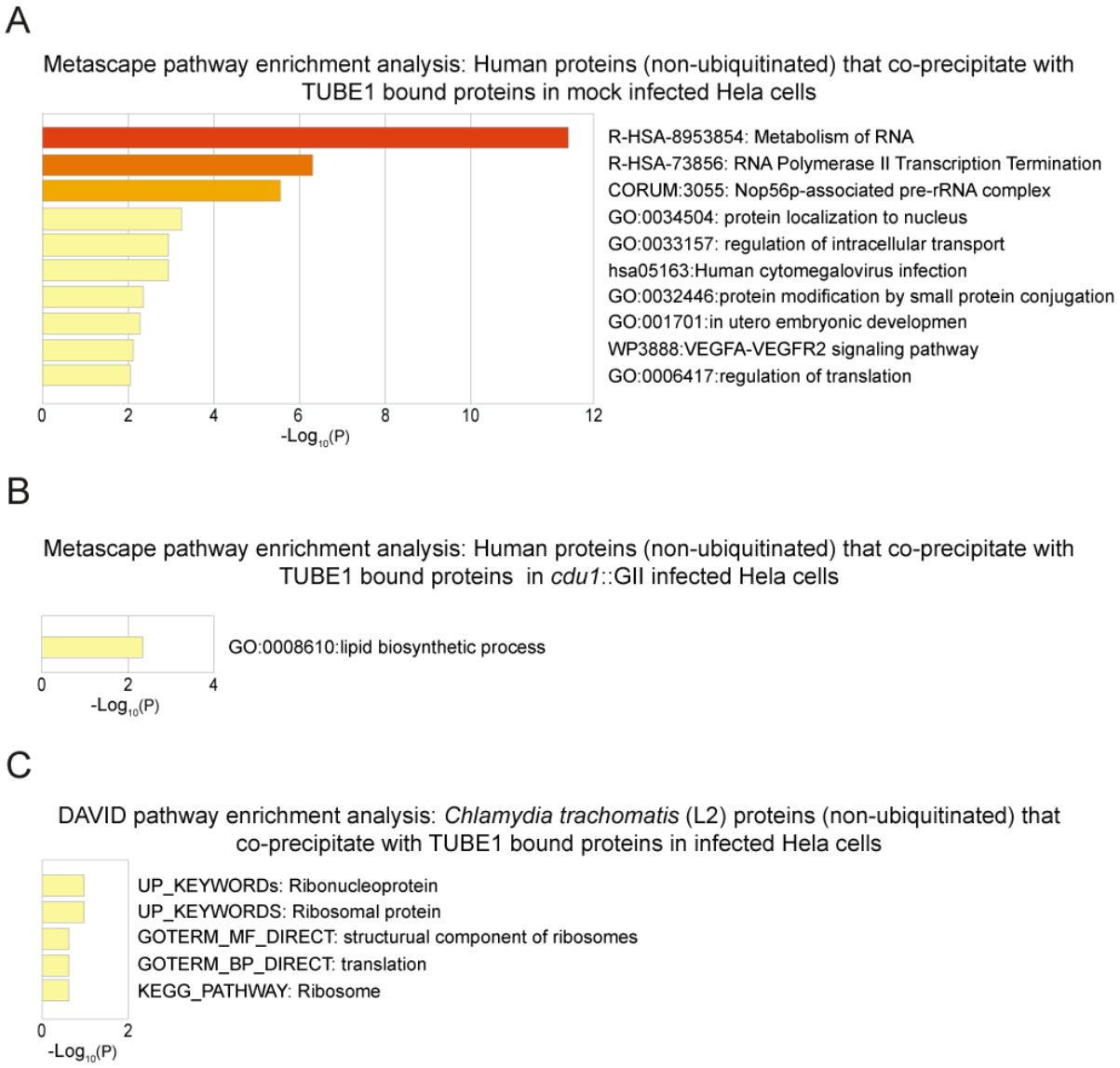

Supplementary Figure 4

Pathway enrichment analysis of human and Ct proteins that co-precipitate (non ubiquitinated) with TUBE1 bound proteins. (A) Metascape functional enrichment analysis of human co-precipitating proteins in mock infected HeLa cells. **(B)** Metascape functional enrichment analysis of human co-precipitating proteins in *cdu1* null infected HeLa cells. **(C)** DAVID pathway enrichment analysis of Ct co-precipitating proteins enriched in infected (L2 and *cdu1* null) HeLa cells.

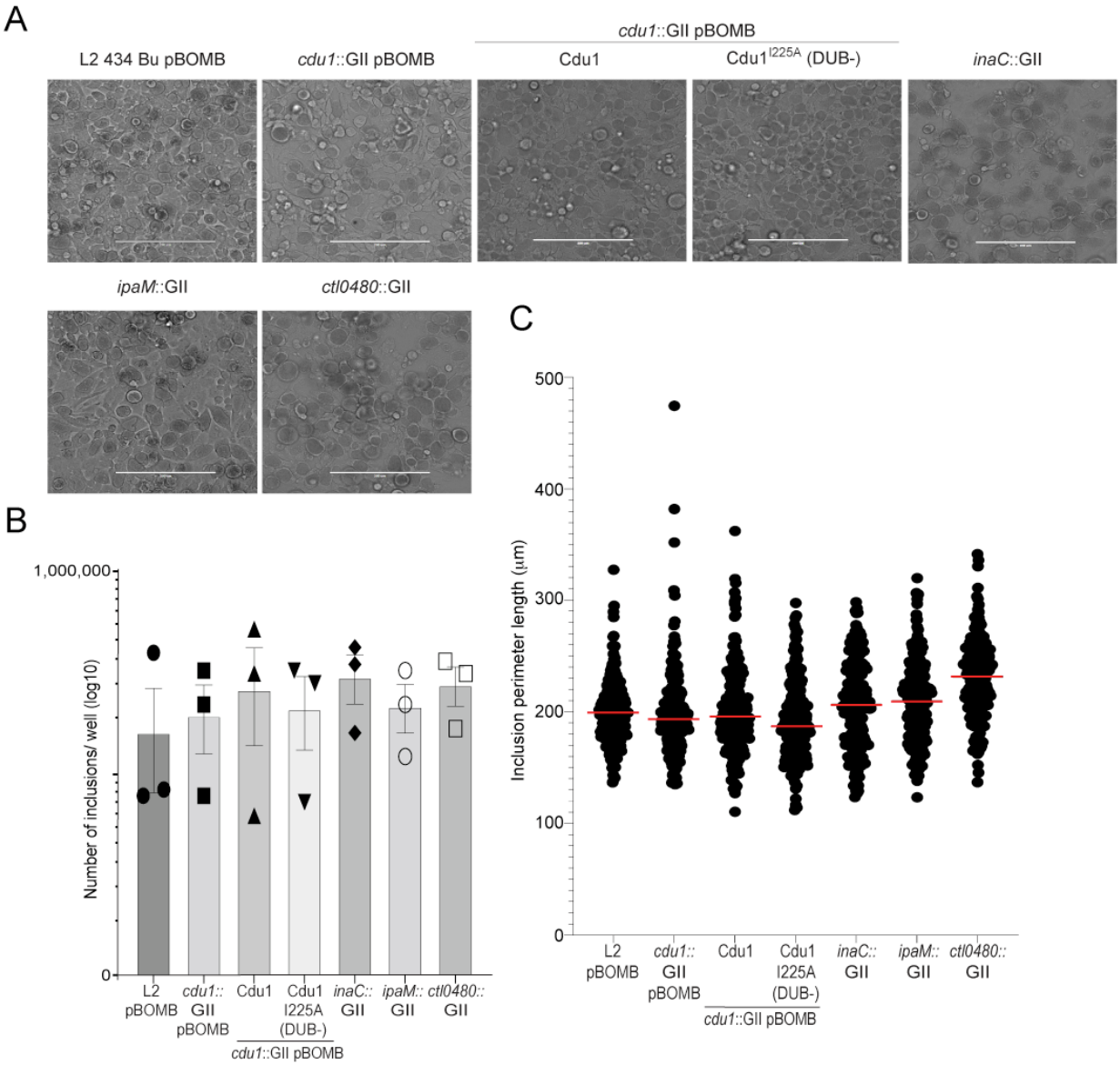

Supplementary Figure 5

The number of inclusions and the size of inclusions in *cdu1* null, *inaC* null, *ipaM* null, and *ctl0480* null strains are similar across each strain (A) Representative images of inclusions in infected HeLa cell monolayers at 48 hpi. Scale bar: 200 µm **(B)** Quantification of the number of inclusions in infected HeLa cell monolayers. **(C)** Quantification of inclusion size.